NASA Contractor Report 187513

ICASE Report No. 91–11

ICASE

MULTIGRID SOLUTION OF COMPRESSIBLE TURBULENT FLOW ON UNSTRUCTURED MESHES USING A TWO-EQUATION MODEL

D. J. Mavriplis
L. Martinelli

Contract No. NAS1–18605
January 1991

Institute for Computer Applications in Science and Engineering
NASA Langley Research Center
Hampton, Virginia 23665–5225

Operated by the Universities Space Research Association

National Aeronautics and
Space Administration

Langley Research Center
Hampton, Virginia 23665-5225

MULTIGRID SOLUTION OF COMPRESSIBLE TURBULENT FLOW ON UNSTRUCTURED MESHES USING A TWO-EQUATION MODEL

D. J. Mavriplis

Institute for Computer Applications in Science and Engineering
NASA Langley Research Center

L. Martinelli

Princeton University
Princeton, New Jersey

ABSTRACT

The steady-state solution of the system of equations consisting of the full Navier-Stokes equations and two turbulence equations has been obtained using a multigrid strategy on unstructured meshes. The flow equations and turbulence equations are solved in a loosely coupled manner. The flow equations are advanced in time using a multi-stage Runge-Kutta time stepping scheme with a stability bound local time-step, while the turbulence equations are advanced in a point-implicit scheme with a time-step which guarantees stability and positivity. Low Reynolds number modifications to the original two-equation model are incorporated in a manner which results in well behaved equations for arbitrarily small wall distances. A variety of aerodynamic flows are solved for, initializing all quantities with uniform freestream values. Rapid and uniform convergence rates for the flow and turbulence equations are observed.

This research was supported under the National Aeronautics and Space Administration under NASA Contract No. NAS1-18605 while the author was in residence at the Institute for Computer Applications in Science and Engineering (ICASE), NASA Langley Research Center, Hampton, VA 23665.

1. INTRODUCTION

The use of unstructured meshes has become more widespread in recent years due to the ease with which complex geometries can be handled and the possibility of enhancing the solution accuracy and efficiency through adaptive meshing techniques. To date, most of the successes of unstructured mesh techniques have been in computing inviscid flows in two and three dimensions over arbitrary geometries. However, more recently, solutions of the Navier-Stokes equations on unstructured meshes have been reported [1,2,3,4,5]. The main obstacles to efficiently computing high-Reynolds-number flows on unstructured meshes are due to the required grid stretching and the turbulence model. For high-Reynolds-number flows over streamlined bodies, viscous effects are confined to thin boundary-layer and wake regions, which can only be resolved efficiently using high aspect ratio elements. One approach [3,5] is to fit a thin local mesh of structured high aspect ratio quadrilaterals in the viscous regions, and fill the remainder of the domain with an unstructured mesh. The other approach consists of filling the entire domain with an unstructured mesh which contains highly stretched triangular elements in the viscous regions [4]. In this work, the latter approach has been pursued, in the interest of developing a more general method capable of dealing with a wider variety of flows, such as flows with confluent boundary layers, or mixing wakes, and also to enable the straight-forward implementation of adaptive meshing techniques throughout all regions of the flow-field. The numerical scheme must therefore be formulated such that the accuracy and convergence are not seriously affected by the presence of highly stretched triangular elements.

The most commonly employed turbulence models for compressible flow calculations are of the algebraic mixing-length type [6]. These models have been shown to produce good results for attached turbulent boundary layers and mildly separated flows using structured meshes, and have also been implemented for non-trivial geometries on unstructured meshes [7]. Although such models can be made inexpensive and computationally robust even in the context of unstructured meshes, they lack the generality required for dealing with completely arbitrary geometries, and their ability in predicting flows with multiple confluent shear layers and large amounts of separation is at best limited. Two equation models, on the other hand, offer the possibility of dealing with the more complicated flows which are often associated with the complex geometries for which unstructured meshes are so well suited. In principle, the implementation of such models on unstructured meshes can be accomplished in a straight-forward fashion, simply by discretizing and integrating the turbulence equations in a manner analogous to that employed for the mean flow equations. However, field-equation turbulence models have often proved to be extremely difficult to integrate to steady-state, exhibiting stiff or unstable numerical behavior in regions very close to the wall, as well as in the far-field. The use of multigrid to solve the turbulence equations has recently been reported by several authors [8,9], using a Ni-type scheme on structured meshes. In this work, a multigrid strategy which has previously been developed for the Euler and Navier-Stokes equations on unstructured meshes [4,10] is extended to solve for the two turbulence equations as well.

2. GOVERNING EQUATIONS

The governing equations are obtained by Favre averaging the Navier-Stokes equations, and modeling the Reynolds stress and heat flux terms by the Boussinesq assumption. In conservative form, these equations are written as

$$\frac{\partial w}{\partial t} + \frac{\partial f_c}{\partial x} + \frac{\partial g_c}{\partial y} = \frac{\partial f_v}{\partial x} + \frac{\partial g_v}{\partial y} \tag{1}$$

where w is the solution vector and f_c and g_c are the cartesian components of the convective fluxes

$$w = \begin{bmatrix} \rho \\ \rho u \\ \rho v \\ \rho E \end{bmatrix} \quad f_c = \begin{bmatrix} \rho u \\ \rho u^2 + p \\ \rho uv \\ \rho uE + up \end{bmatrix} \quad g_c = \begin{bmatrix} \rho v \\ \rho vu \\ \rho v^2 + p \\ \rho vE + vp \end{bmatrix} \tag{2}$$

In the above equations, ρ represents the fluid density, u and v the x and y components of fluid velocity, E the total energy, and p is the pressure which can be calculated from the equation of state of a perfect gas

$$p = (\gamma-1)\rho\left[E - \frac{(u^2+v^2)}{2}\right] \tag{3}$$

The viscous fluxes f_v and g_v are given by

$$f_v = \begin{bmatrix} 0 \\ \sigma_{xx} \\ \sigma_{xy} \\ u\sigma_{xx} + v\sigma_{xy} - q_x \end{bmatrix} \quad g_v = \begin{bmatrix} 0 \\ \sigma_{xy} \\ \sigma_{yy} \\ u\sigma_{yx} + v\sigma_{yy} - q_y \end{bmatrix} \tag{4}$$

where σ represents the stress tensor, and $\mathbf{q}$ the heat flux vector, which are given by

$$\sigma_{xx} = 2(\mu + \mu_t)u_x - \frac{2}{3}(\mu + \mu_t)(u_x+v_y) - \frac{2}{3}\rho k \tag{5}$$

$$\sigma_{yy} = 2(\mu + \mu_t)v_y - \frac{2}{3}(\mu + \mu_t)(u_x+v_y) - \frac{2}{3}\rho k \tag{6}$$

$$\sigma_{xy} = \sigma_{yx} = (\mu + \mu_t)(u_y+v_x) \tag{7}$$

$$q_x = -\frac{\gamma}{\gamma-1}\left(\frac{\mu}{Pr} + \frac{\mu_t}{Pr_t}\right)\frac{\partial \frac{p}{\rho}}{\partial x} \tag{8}$$

$$q_y = -\frac{\gamma}{\gamma-1}\left(\frac{\mu}{Pr} + \frac{\mu_t}{Pr_t}\right)\frac{\partial \frac{p}{\rho}}{\partial y} \tag{9}$$

μ represents the molecular viscosity, and μ_t denotes the turbulent eddy viscosity, which must be computed by a suitable turbulence model. Pr is the laminar Prandtl number, which is taken as 0.7 for air, Pr_t is the turbulent Prandtl number, taken as 0.9, and γ is the ratio of specific heats of the fluid.

The high Reynolds number k–ε turbulence model originally described by Launder and Spalding [11], can similarly be written as

$$\frac{\partial w}{\partial t} + \frac{\partial f_c}{\partial x} + \frac{\partial g_c}{\partial y} = \frac{\partial f_v}{\partial x} + \frac{\partial g_v}{\partial y} + h \tag{10}$$

where w, f_c and g_c are now given by

$$w = \begin{bmatrix} \rho k \\ \rho \varepsilon \end{bmatrix} \quad f_c = \begin{bmatrix} \rho uk \\ \rho u\varepsilon \end{bmatrix} \quad g_c = \begin{bmatrix} \rho vk \\ \rho v\varepsilon \end{bmatrix} \tag{11}$$

The diffusive fluxes f_v and g_v are given by

$$f_v = \begin{bmatrix} \frac{\mu_t}{\sigma_k}\frac{\partial k}{\partial x} \\ \frac{\mu_t}{\sigma_\varepsilon}\frac{\partial \varepsilon}{\partial x} \end{bmatrix} \quad g_v = \begin{bmatrix} \frac{\mu_t}{\sigma_k}\frac{\partial k}{\partial y} \\ \frac{\mu_t}{\sigma_\varepsilon}\frac{\partial \varepsilon}{\partial y} \end{bmatrix} \tag{12}$$

and the source term h is given by

$$h = \begin{bmatrix} \mu_t P - \frac{2}{3} S \rho k - \rho \varepsilon \\ C_1 \frac{\varepsilon}{k} (\mu_t P - \frac{2}{3} S \rho k) - C_2 \rho \frac{\varepsilon^2}{k} \end{bmatrix} \tag{13}$$

where the production term P and the term S in two dimensions are given by

$$P = \frac{4}{3}(u_x^2 + v_y^2 - u_x v_y) + (u_y + v_x)^2 \tag{14}$$

$$S = u_x + v_y$$

The eddy viscosity is calculated as

$$\mu_t = \frac{\rho C_\mu k^2}{\varepsilon} \tag{15}$$

and k also appears in the normal stresses in equation (5). The constants appearing in the above equations are given the standard values recommended in [11], i.e.

$$C_\mu = 0.09 \qquad \sigma_k = 1.0 \qquad \sigma_\varepsilon = 1.3 \qquad C_1 = 1.44 \qquad C_2 = 1.92 \tag{16}$$

These equations are coupled to the governing equations for the mean flow and exhibit a similar structure. Therefore, a single system of equations which simultaneously governs the flow and turbulence quantities may be written as

$$\frac{\partial w}{\partial t} + \frac{\partial f_c}{\partial x} + \frac{\partial g_c}{\partial y} = \frac{\partial f_v}{\partial x} + \frac{\partial g_v}{\partial y} + h \tag{17}$$

where the solution vector and the source term are now given by

$$w = \begin{bmatrix} \rho \\ \rho u \\ \rho v \\ \rho E \\ \rho k \\ \rho \varepsilon \end{bmatrix} \qquad h = \begin{bmatrix} 0 \\ 0 \\ 0 \\ 0 \\ \mu_t P - \frac{2}{3} S \rho k - \rho \varepsilon \\ C_1 \frac{\varepsilon}{k} (\mu_t P - \frac{2}{3} S \rho k) - C_2 \rho \frac{\varepsilon^2}{k} \end{bmatrix} \tag{18}$$

and the flux definitions follow from equations (2),(4),(11), and (12).

The solution procedure consists of discretizing these equations in space on an unstructured mesh, and then integrating the discretized equations in time until the steady-state solution is obtained. The basic strategy pursued in this work involves the use of a finite-element Galerkin discretization technique, in conjunction with an unstructured multigrid integration technique to solve for the steady-state. Although all six equations of the governing system are solved simultaneously in the multigrid strategy, the flow equations are only loosely coupled to the turbulence equations (through the value of μ_t), and we choose to employ somewhat different base grid solvers for the flow equations and the turbulence equations.

3. SPATIAL DISCRETIZATION

The equations governing the mean flow are discretized using a Galerkin finite-element approach [4]. The flow variables are stored at the vertices of the triangles. The convective fluxes are computed at the vertices of the triangles and assumed to vary linearly over the triangular elements. For the viscous terms, the flow variables themselves are assumed to vary linearly over the triangular elements of the mesh, and the required velocity gradients in the expression for the viscous stresses are thus computed at the centers of the triangular elements. Additional artificial dissipation terms are required to ensure the stability of the convective

terms and these are constructed as a blend of a Laplacian and biharmonic operators in the conserved variables, designed to ensure second-order accuracy throughout the flow-field, except in the vicinity of a shock where first-order accuracy is recovered. For the turbulence equations, the diffusive terms are similarly discretized using a Galerkin finite-element approach, assuming linear variations of the conserved variables over the triangular elements. The velocity gradients in the source terms are also constructed assuming linear elements. The convective terms, however, are constructed using first-order upwinding. Although only first-order accurate, this approach is employed since it helps ensure stability and positivity of the conserved variables throughout the integration procedure, as will be shown. Furthermore, in regions where convection is small compared to the diffusion terms or the source terms, such as in the logarithmic law of the wall region, the scheme reverts to second order accuracy. In future work however, a second-order accurate implementation of the convective terms may be pursued.

4. INTEGRATION SCHEME

The discretized mean flow equations are integrated in time using an explicit five-stage Runge-Kutta time-stepping scheme, where the convective terms are evaluated at every stage, and the dissipative terms are only evaluated at the first, third and fifth stages. This scheme, which has previously been described [4,12], has been particularly devised to ensure rapid damping of high-frequency errors, and is thus well suited to drive the multigrid algorithm. Convergence is accelerated by the use of local time-stepping, and implicit residual averaging. In principle, the turbulence equations may be integrated in time using the same explicit scheme. However, the presence of source terms imposes a further time-step restriction. If the flow equations and turbulence equations are integrated in a fully coupled manner, the minimum local time-step from the flow and turbulence equations must be employed. In regions where the source terms dominate, this may lead to slow convergence. If, on the other hand, the flow equations and turbulence equations are integrated in an uncoupled explicit manner, the turbulence equations may significantly lag the flow equations and thus inhibit convergence to the steady-state solution. In order to advance the turbulence quantities at the same rate as the flow equations, the source terms must be treated implicitly. However, rather than simply treat the source terms implicitly, the system of turbulence equations is integrated in a point-implicit manner. Thus we rewrite the discretized turbulence equations as

$$\frac{\Delta w_i}{\Delta t} = R(w_i) + H(w_i) \tag{19}$$

where $R(w_i)$ represents the discretized convective and diffusive terms, which depend on the values of w at i and at neighboring nodes, and $H(w_i)$ represents the discretized source terms, which only depend on the values of w at i. The above equation is then linearized about the values at i which, upon solving for Δw_i yields

$$\Delta w_i = \left[\frac{1}{\Delta t} - \frac{\partial R}{\partial w} - \frac{\partial H}{\partial w}\right]^{-1}\left[R(w_i) + H(w_i)\right] \tag{20}$$

The Runge-Kutta scheme described above is now replaced by a multi-stage implicit scheme, where the qth stage is given by

$$w^{(q)} = w^{(0)} + \left[\frac{1}{\alpha_q \Delta t} - \frac{\partial R}{\partial w} - \frac{\partial H}{\partial w}\right]^{-1}\left[R^{(q-1)}(w_i) + H^{(q-1)}(w_i)\right] \tag{21}$$

where the α_q denote the Runge-Kutta coefficients for the qth stage, and Δt is the local time step. In this manner, the high-frequency damping characteristics of the original scheme are approximated, while the time-step restriction due to the source terms is alleviated. The precise

value of the local time-step Δt employed is one which guarantees stability as well as positivity of the turbulence quantities.

5. STABILITY AND POSITIVITY CONSIDERATIONS

One method to guarantee stability of the system is to ensure that the matrix to be inverted is diagonally dominant. This is not a necessary condition for stability, although it is sufficient. This can obviously be achieved by choosing Δt to be sufficiently small. However, the reason for employing a point-implicit approach now becomes apparent. Since the two turbulence equations are only coupled through their source terms, the $\frac{\partial R}{\partial w}$ matrix is diagonal. The contribution from the diffusive terms is strictly negative, as well as that from the first-order upwinded convective terms. Hence, these terms, when subtracted from the diagonal of the matrix to be inverted, increase the diagonal dominance, and hence permit the use of a larger time-step. The maximum value of Δt is found by equating each diagonal element to its corresponding off-diagonal element in the coefficient matrix. The actual value employed for the time-step is taken as the minimum between the two values obtained by the diagonal dominance test, and the value determined by local stability analysis for an explicit scheme in the absence of source terms.

Physically, k and ε represent quantities which must remain non-negative. Thus a further time-step restriction is required to ensure positivity. For a simple 2x2 system, this can easily be derived analytically. Thus, we require that the new update to the turbulence variables be such that

$$w + \Delta w > \alpha w \qquad 0 < \alpha < 1$$

or, when $\Delta w < 0$

$$|\Delta w| < (1-\alpha)\, w \qquad 0 < \alpha < 1 \tag{22}$$

Substituting into equation (20), and using Cramer's rule to evaluate the inverse of the 2x2 matrix, we obtain two quadratic inequalities for Δt, i.e. one for positivity of k, and one for ε. The time step is then limited by the smallest positive root of the two quadratic equations.

6. MULTIGRID STRATEGY AND STEADY-STATE CONSIDERATIONS FOR THE $k-\varepsilon$ EQUATIONS

A multigrid strategy is employed to accelerate the solution of the system of mean flow and turbulence equations to steady-state. In the context of unstructured meshes, multigrid may be applied by generating a sequence of non-nested coarse and fine meshes, and transferring the variables, residuals and corrections back and forth between the various meshes using linear interpolation. The patterns for interpolating between non-nested unstructured meshes are determined in a preprocessing stage, using an efficient search algorithm. The present multigrid strategy has previously been described in detail for the Euler and Navier-Stokes equations [4,10], and thus will not be repeated here. In previous multigrid applications for turbulent flows using algebraic models on structured and unstructured meshes [7,13], the eddy viscosities are only computed on the finest grid, and interpolated to the coarser meshes. Since the eddy viscosity represents the main coupling between the flow equations and the turbulence equations, a similar approach has been adopted in the present context, thus ensuring a more accurate representation of this quantity on all grid levels. However, since the eddy viscosity is only computed on the finest grid, it is effectively held constant throughout an entire multigrid cycle, and the source terms must be linearized accordingly. Making use of equations (11) and (13), the linearization of the source terms on all grids is therefore taken as

$$\frac{\partial H}{\partial w} = \begin{bmatrix} -\frac{2}{3}S & -1 \\ \frac{-C_1\mu_t P}{\rho}\frac{\varepsilon}{k^2} + C_2\frac{\varepsilon^2}{k^2} & C_1\left[\frac{\mu_t P}{\rho k} - \frac{2}{3}S\right] - 2C_2\frac{\varepsilon}{k} \end{bmatrix} \tag{23}$$

At this point it is worth commenting on what types of errors may be expected to be handled efficiently by a multigrid strategy. Multigrid is an effective device for relieving the spatial stiffness associated with a set of discretized equations, which is achieved by time-stepping on coarser grids. The turbulence equations contain spatial terms such as convection and diffusion, but the source terms are purely local terms. In fact, in the absence of convection and diffusion, the equations become completely uncoupled in space, and a properly formulated multigrid algorithm should yield vanishingly small corrections in such a case. Thus, it is important for the base grid solver to efficiently eliminate errors associated with these terms. From another point of view, if a purely explicit scheme were employed, a time-step restriction would arise from the convection, diffusion and source terms. While the first two restrictions are relaxed when going to coarser grids, the latter remains the same on all grid levels, effectively preventing the use of large time-steps on coarse grids and severly limiting the overall rate of convergence. The use of a point-implicit scheme, therefore, relieves any such restrictions, and results in overall convergence rates similar to that achieved with the mean flow equations.

At steady-state, the turbulence equations do not necessarily exhibit a unique solution. In regions where the production term $\mu_t P$ vanishes, $k = 0$, $\varepsilon = 0$ is an obvious solution which can be found by inspection of equations (10) and (13). However, the eddy viscosity, which is given by equation (15), becomes a ratio of two vanishing quantities, and is thus undefined. The time dependent turbulence equations however, are not ill-posed. On the contrary, the value of the constant C_2 has been carefully chosen to ensure that k, ε and μ_t all vanish asymptotically for an isotropic decaying turbulence. For an isotropic turbulence, all spatial terms as well as the production term vanish, and equations (10) and (13) reduce to

$$\begin{aligned} \frac{dk}{dt} &= -\varepsilon \\ \frac{d\varepsilon}{dt} &= -C_2\frac{\varepsilon^2}{k} \end{aligned} \tag{24}$$

Solution of this system yields the following asymptotic behavior

$$k \approx t^{-\frac{1}{C_2-1}} \qquad \varepsilon \approx t^{-\frac{C_2}{C_2-1}} \qquad \frac{k^2}{\varepsilon} \approx t^{\frac{C_2-2}{C_2-1}} \qquad t \longrightarrow \infty \tag{25}$$

which, for the current value of $1 < C_2 < 2$ indicates that all quantities vanish for large t. Hence, in order to converge to the appropriate steady-state solution, it is important for any numerical scheme to respect the relative asymptotic time behavior of k and ε throughout the convergence process. For the base grid solver, this is achieved by employing the maximum time-step for the system of two turbulence equations which ensures stability and positivity; letting k or ε become negative, or taking too large time steps and subsequently limiting the updated values of k or ε invariably leads to unrealistic values of μ_t in the far-field. Within the multigrid strategy, corrections interpolated back from the coarser grids may cause k or ε to become negative. Rather than limit these corrections, they are simply omitted at any point where positivity cannot otherwise be guaranteed. In this manner, the (point-wise) time consistency is not violated, and the overall effect is simply to lag such points by the effective coarse grid time step. An alternate approach would be to recompute the coarse grid corrections employing a smaller time step which guarantees positivity. However, due to the recursive

nature of multigrid, this represents a non-trivial task.

7. BOUNDARY AND INITIAL CONDITIONS

The derivation of the above turbulence transport equations is made under the hypothesis of a large Reynolds number flow. Thus, in regions close to the wall, such as in the viscous sublayer where molecular effects become important, these equations are not valid. In order to avoid integrating the turbulence equations in these region we make use of wall functions. In this approach, the governing equations for the flow and the turbulence are integrated up to a distance $y = y_n$ away from the wall. The flow in the remaining region $0 < y < y_n$ is assumed to obey the law of the wall i.e.

$$\frac{U}{U_\tau} = \frac{1}{\kappa}\ln\frac{\rho U_\tau y}{\mu} + 5.5 \qquad (26)$$

At each time-step in the solution procedure of the governing equations, an estimate of the velocity U at $y = y_n$ is obtained. From this, the value of the wall shear stress can be obtained by solving equation (26) implicitly for U_τ (using a Newton-Raphson method). This estimate of the wall shear stress is then employed as a boundary condition on the momentum equation for the mean flow, and results in Dirichlet wall boundary conditions for k and ε. In practice the point $y = y_n$ is very close to the wall so that it may be approximately placed on the wall, and the boundary conditions at $y = y_n$ may be imposed at the wall surface. For the momentum equation, this results in a wall slip velocity $U = U(y_n)$.

In the far-field, k and ε are assigned freestream values at inflow boundaries, and simple extrapolation is employed at outflow boundaries. Initial conditions on k and ε are obtained by imposing a level of freestream turbulence from which k is determined, and ε is evaluated from equation (15) in order to produce a low value of freestream eddy viscosity ($\mu_t < 1$). However, since the present formulation results in a small value of μ_t in all regions of the flow field where production is negligible, the converged solution is relatively insensitive to the initial values of k and ε. The mean flow equations are initialized using uniform freestream flow conditions, and applying the tangential slip velocity boundary condition (as for an inviscid flow). Throughout the integration process, the wall shear stress obtained from equation (26), which is fed back into the momentum equation, retards the flow near the wall, thus creating a boundary layer profile.

8. RESULTS USING WALL FUNCTIONS

Two attached flow cases have been computed using the multigrid implementation of the high-Reynolds-number turbulence model described above. The first case consists of transonic flow past an RAE 2822 airfoil. The freestream Mach number is 0.729, the incidence is 2.31 degrees, and the Reynolds number is 6.5 million. This case (case 6) has been well documented both experimentally [14] and computationally [7,13,15] on structured and unstructured meshes. The mesh employed for this case is depicted in Figure 1. It contains 12,823 vertices and exhibits a normal spacing of 10^{-4} chords at the airfoil surface, which positions the first point off the wall in the logarithmic law of the wall region. The computed Mach contours for this case are shown in Figure 2, while the resulting eddy viscosity distribution is given in Figure 3. A smooth distribution of eddy viscosity throughout the boundary-layer and wake regions, and vanishingly small values in the inviscid regions of flow are observed. The computed surface pressure distribution is compared with experimental data [14] in Figure 4, showing good overall agreement. The convergence rate of the system of equations is depicted in Figure 5, by plotting the RMS average of the density residual, and the residual of ρk throughout the flow

field, versus the number of multigrid cycles. As can be seen, the flow equations and turbulence equations converge with the same asymptotic rates. The residuals are reduced by roughly 6 orders of magnitude over 200 cycles, yielding an overall convergence rate of 0.93

The second case involves flow over a high-lifting four-element airfoil. This case is useful in demonstrating the complex geometries and resulting flow-fields which can be handled by the present methodology. The mesh employed is depicted in Figure 6. It contains a total of 51,100 vertices and a normal spacing of $2x10^{-4}$ chords off the wall for each airfoil element. The computed Mach contours are shown in Figure 7, while the resulting eddy viscosity distribution is given in Figure 8. The ease with which multiple wakes and confluent boundary layers may be handled by the present approach is evident from the figures. The computed surface pressure distribution is seen to compare favorably with experimental wind-tunnel data from [16] in Figure 9. It should however be pointed out that such favorable agreement is in large part due to the attached nature of the flow. The multigrid convergence rates of the density equation and the k equation are depicted in Figure 10, where both equations are seen to achieve approximately the same asymptotic rates, decreasing by 4 orders of magnitude over 300 cycles.

9. LOW REYNOLDS NUMBER TURBULENCE MODEL MODIFICATIONS

While the use of the high-Reynolds-number turbulence equations in conjunction with wall functions is useful for a large class of wall bounded flows, it is nevertheless limited to flows where a logarithmic law of the wall region exists, and is thus strictly not valid for separated flows. An alternative approach is to modify the turbulence equations in order to account for low-Reynolds-number effects. Many such modifications have been proposed over the years with varying degrees of success [17]. One common feature of all such modifications is that they have proved exceedingly difficult to integrate numerically very close to the wall. The aim of the present work is to develop an efficient and robust technique for integrating such models, rather than reformulating or advocating any one model in particular. With this in mind, we chose to implement the simplest possible low-Reynolds-number model that has been demonstrated to produce good results for simple problems, with possible extensions to more complex models should the original version prove inadequate for more complicated flows. To this end, the modifications proposed by Speziale, Abid and Anderson [18] have been implemented. The modified turbulence equations, now given in vector form, can be written as

$$\frac{\partial \rho k}{\partial t} + u.\nabla(\rho k) = \nabla.\left[(\mu + \frac{\mu_t}{s_k})\nabla k\right] + \mu_t P - \frac{2}{3}S\rho k - \rho\varepsilon$$

$$\frac{\partial \rho \varepsilon}{\partial t} + u.\nabla(\rho \varepsilon) = \nabla.\left[(\mu + \frac{\mu_t}{s_\varepsilon})\nabla \varepsilon\right] + C_1(\mu_t P - \frac{2}{3}S\rho k)\frac{\varepsilon}{k} - C_2 f_2 \rho \frac{\varepsilon^2}{k}$$

$$\mu_t = \frac{\rho C_\mu f_\mu k^2}{\varepsilon} \tag{27}$$

$$f_\mu = (1 + \frac{3.45}{\sqrt{Re_t}}) \tanh(\frac{-y^+}{70})$$

$$f_2 = [\,1 - \exp(\frac{-y^+}{4.9})\,]^2$$

with boundary conditions at the wall given by

$$k = 0 \tag{28}$$

$$\varepsilon = \frac{\mu}{\rho}\frac{\partial^2 k}{\partial y^2}$$

and employing the following values for the constants

$$C_\mu = 0.09 \qquad \sigma_k = 1.36 \qquad \sigma_\varepsilon = 1.36 \qquad C_1 = 1.44 \qquad C_2 = 1.83\ [1 - \frac{2}{9}\exp(\frac{-Re_t}{6})^2\ ]$$

where $Re_t = \rho\frac{k^2}{\mu\varepsilon}$ is the turbulence Reynolds number. As can be seen, no extra source terms are introduced, and only two damping functions are required. This model is similar in form to the Lam-Bremhorst model [19], with the notable difference that all damping functions depend solely on y^+. The evaluation of such functions requires the knowledge of the distance of each point from the closest wall. In the context of unstructured meshes, this information can be constructed through the use of a generalized distance function, as outlined by Barth [20]. As with most low-Reynolds-number turbulence models, the current form of the model has been reported to be extremely stiff in near-wall regions, generally requiring the prescription of initial profiles in k and ε in order to guarantee convergence to steady-state. Such techniques are considered impractical for complex aerodynamic flows, and thus a more robust solution strategy has been pursued. The difficulties associated with the near-wall regions can be assessed by inspection of equations (27). When the wall boundary condition $k = 0$ is substituted into the ε equation, it is seen to result in a singularity, since k appears in the denominator of this equation. Since f_2 also vanishes at the wall, this singularity is in principle removable. However, the numerical integration of the ε equation in its present form will only be well behaved if f_2 and k have the same asymptotic behavior near the wall throughout the integration procedure, thus the need for startup profiles. The approach taken in this work is to remove the singularity by solving for a new variable defined as

$$k = \tilde{k}\, f_2 \qquad or \qquad \tilde{k} = \frac{k}{f_2} \tag{29}$$

Upon substituting this expression into equation (27), and using the chain rule to evaluate the gradient operators, one obtains the new set of equations

$$\begin{aligned} \frac{\partial \rho\tilde{k}}{\partial t} + u.\nabla(\rho\tilde{k}) &= \nabla.\left[(\mu + \frac{\mu_t}{s_k})\nabla\tilde{k}\right] \\ &+ \frac{1}{f_2}\left[\ \mu_t P - \frac{2}{3}S\rho\tilde{k}f_2 - \rho\varepsilon\ \right] \\ &+ \frac{1}{f_2}\left[\ \left[\ \nabla(\mu + \frac{\mu_t}{s_k}) - \rho u\ \right].\nabla f_2 + (\mu + \frac{\mu_t}{s_k})\nabla^2 f_2\ \right]\tilde{k} \\ &+ \frac{1}{f_2}\left[\ 2\ (\mu + \frac{\mu_t}{s_k})\ \nabla f_2 .\nabla\tilde{k}\ \right] \end{aligned} \tag{30}$$

$$\frac{\partial \rho\varepsilon}{\partial t} + u.\nabla(\rho\varepsilon) = \nabla.\left[(\mu + \frac{\mu_t}{s_\varepsilon})\nabla\varepsilon\right] + C_1\frac{\mu_t P}{f_2}\frac{\varepsilon}{\tilde{k}} - \frac{2}{3}C_1 S\rho\varepsilon - C_2\rho\frac{\varepsilon^2}{\tilde{k}}$$

While the $\tilde{k}$ equation now looks rather complicated, the new terms are only significant in the region $f_2 \ll 1$, and in fact, although all terms have been included, only the $\tilde{k}\nabla^2 f_2$ term has been found to have a significant effect on the overall solution. At the wall, we have

$$f_2 = 0, \qquad \nabla f_2 = 0, \qquad \nabla^2 f_2 > 0$$

as well as

$$\mu_t = 0 \qquad P = 0 \qquad S = 0 \qquad u = 0$$

The boundary condition $k = 0$ implies $\tilde{k}$ bounded at the wall. Since f_2 which appears as a denominator in the right-hand side of the $\tilde{k}$ equation vanishes, we require the non vanishing terms in the numerator to sum to zero, thus yielding the condition

$$\tilde{k} = \frac{\rho\varepsilon}{\mu\,\nabla^2 f_2} \tag{31}$$

Upon substituting this expression into the ε equation, with $u = 0$, $\mu_t = 0$, and $S = 0$ one obtains a modified Helmoltz equation for ε at the wall in the steady-state

$$\nabla\left[\mu \nabla\varepsilon\right] - C_2 \mu \nabla^2 f_2 \varepsilon = 0 \tag{32}$$

This equation is well behaved and simple to integrate numerically. The boundary condition employed for ε is taken to be

$$\frac{\partial \varepsilon}{\partial y} = 0 \tag{33}$$

While it is realized that this condition may not be entirely accurate at the wall [21], it is used at this initial stage for simplicity and may be modified in further work.

In regions removed from the wall, the ε equation remains well behaved. The k equation on the other hand contains the source term $\tilde{k}\nabla^2 f_2$. $\nabla^2 f_2$, which can be approximated as $\frac{d^2 f_2}{dy^2}$ has the following properties

$$\begin{aligned} \nabla^2 f_2 &> 0 \qquad & y^+ &< 3.4 \\ \nabla^2 f_2 &< 0 \qquad & y^+ &> 3.4 \end{aligned} \tag{34}$$

where $y^+ = 3.4$ represents the point of inflection in the f_2 function. In regions where $\nabla^2 f_2$ is negative or zero, the k equation is well behaved. However, $\nabla^2 f_2$ large and positive represents a growing source term, which can be numerically unstable. However, since the point $y^+ = 3.4$ is very close to the wall, and within the laminar sublayer, k can be approximated by the relation

$$k^+ = constant \cdot y^{+2} \tag{35}$$

or

$$\tilde{k} = \tilde{k}_{wall} \frac{y^{+2}}{[1 - \exp(\frac{-y^+}{4.9})]^2} \tag{36}$$

which from direct simulations [22], is generally known to be valid up to $y^+ = 10$. Finally, in regions far away from the wall, the damping functions become unity, their derivatives all vanish, and the original high-Reynolds-number equations are recovered, albeit with the new values of the constants advocated in [18]. Thus, in summary, the ε equation given in the form (30) is employed throughout the entire flow-field, except at the wall, where the form (32) is used. For the $\tilde{k}$ equation, the form given by equation (30) is employed from the far-field up to $y^+ = 3.4$, which is within the laminar sublayer. Below this value of y^+, equation (36) is employed with the boundary condition for $\tilde{k}$ given by equation (31).

The multigrid strategy previously described for the high-Reynolds number turbulence equations carries over in a straight-forward manner. The linearization of the source terms is now taken as

$$\frac{\partial H}{\partial w} = \begin{bmatrix} -\frac{2}{3}S + (\mu + \frac{\mu_t}{s_k})\frac{\nabla^2 f_2}{\rho f_2} & -\frac{1}{f_2} \\ C_1 C_\mu f_\mu f_2 P + C_2 \frac{\varepsilon^2}{\tilde{k}^2} & -\frac{2}{3}C_1 S - 2C_2\frac{\varepsilon}{k} \end{bmatrix} \tag{37}$$

where the production term in the ε equation has been simplified by the definition of μ_t in equations (27), in order to remove k from the denominator. The damping functions are evaluated only on the finest grid, and interpolated up to the coarser grids, thus affording a more consistent representation of the equations on all grid levels. A full multigrid strategy is employed, where grid sequencing is used to provide an initial solution for the fine grid. In general, it has been found advantageous to use the high-Reynolds-number model with wall functions on

coarse grids, and the low-Reynolds-number model on the finest grid when grid sequencing, thus rapidly setting up appropriate levels of eddy viscosity on the finest grid.

10. RESULTS

The present implementation of the low-Reynolds-number turbulence model has been employed to compute the turbulent boundary layer over a flat plate, the transonic flow over an RAE 2822 airfoil, and the transonic flow over a two-element airfoil.

The mesh employed to compute the flat plate boundary layer case is depicted in Figure 11. It contains 24 points ahead of the plate, 48 points along the plate in the streamwise direction, and 80 points in the direction normal to the plate. The freestream Mach number is 0.3, and the Reynolds number of the flow, based on the length of the plate is 10 million. The first point normal to the plate is located at a distance of $2x10^{-6}$ plate lengths, which lies in the region $y^+<1$. The resulting velocity profiles are plotted in Figures 12 and 13, both in physical coordinates, and logarithmic wall coordinates, and compared with the well known 1/7th power law distribution, and logarithmic law of the wall profile. The computed skin friction is plotted in Figure 14, versus the experimental data taken from [23]. The resulting distributions of k and ε are shown in Figures 15 and 16. The well known peaks of k and ε are observed, and a non-zero value of ε at the wall is obtained. These distributions are however slightly different from those obtained previously with the same model [18], and may be attributed either to the different boundary condition, or to the near-wall grid resolution. The overall flow quantities are nevertheless well predicted, as shown in Figures 12 through 14.

The transonic flow case over the RAE 2822 airfoil presented in the previous section has been recomputed with the low-Reynolds-number turbulence model (Mach = 0.729, Incidence = 2.31 degrees, Re = 6.5 million). The mesh employed is similar to that shown in Figure 1, except that the normal spacing at the wall is now reduced to $1x10^{-5}$ chords, which results in the first mesh point off the wall in the region $1 < y^+ < 3$ over the entire surface of the airfoil. The computed Mach contours and eddy viscosity contours are similar to those depicted in Figures 2 and 3, except in the near-wall regions, where both quantities vanish rapidly. The computed surface pressure and skin-friction distributions are compared with experimental data in Figures 17 and 18. The computed lift is slightly lower than that predicted with the wall functions and that previously obtained using an algebraic model [7]. At present, it is not clear whether this is due to the actual model formulation, or is associated with the present implementation (artificial dissipation, grid resolution). However, the differences are rather small and the skin friction appears to be well predicted. The convergence of the density equation and the two turbulence equations is depicted in Figure 19, where the residuals are plotted versus the number of multigrid cycles on the finest grid. The flowfield and turbulence equations are all initialized with uniform freestream values, and 25 cycles were performed on the previous coarser grid using wall functions, prior to initializing the solution procedure on the finest grid. Initializing the calculation with freestream values for all equations on the finest grid has also been employed with little degradation in convergence. From Figure 19, all equations are seen to converge at approximately the same rate, resulting in a residual reduction of 4 to 5 orders of magnitude over 300 multigrid cycles.

The final case involves the transonic flow over a two-element airfoil. This case illustrates the ease with which complex geometries and flows with multiple viscous layers may be handled by the present methodology. The mesh employed is depicted in Figure 20. It contains a total of 28,871 vertices, with a normal spacing of $2x10^{-5}$ chords off the wall for each airfoil

element. The freestream Mach number is 0.5, the incidence is 7.5 degrees, and the Reynolds number is 4.5 million. The computed Mach contours and eddy viscosity contours are depicted in Figures 21 and 22. At these conditions, the flow is supercritical and a shock is formed on the upper surface of the slat. A small region of separated flow occurs behind the shock, as can be seen from the skin friction plot of Figure 23. This region of separation has previously been reported in prior calculations using an algebraic turbulence model [7]. The computed surface pressure distribution is seen to compare favorably with experimental wind-tunnel data [24], in Figure 24. The convergence rate for this case is depicted in Figure 25, where the residuals of the density equation and the two turbulence equations are reduced by approximately 3 to 4 orders of magnitude over 300 cycles on the finest grid.

11. CONCLUSION

A multigrid strategy for solving the steady-state high and low-Reynolds number $k - \varepsilon$ turbulence equations has been formulated and implemented on unstructured meshes. A variety of aerodynamic flows have been computed, consistently demonstrating similar convergence rates for the turbulence and flow equations. Initialization of all flow and turbulence quantities may be performed using uniform freestream values. At present, the evaluation of the turbulence terms requires a significant fraction of the overall time within a single time-step. For example, the RAE 2822 supercritical airfoil flow case with the low-Reynolds-number turbulence model requires roughly 2.5 seconds per multigrid cycle on a single processor of the CRAY-YMP supercomputer, which is almost 75% higher than that required by the algebraic model reported previously [7]. However, it is estimated that this can be substantially reduced by assembling the turbulence and flow residuals simultaneously within a single loop. Given the demonstrated convergence rates, the two-equation turbulence model should be competitive in terms of computer resources with algebraic models, while providing much greater flexibility in dealing with complex geometries and flow-fields.

Future work should involve a more thorough investigation of the various two-equation turbulence models and their ability in predicting complex aerodynamic flows, including flows with massive separation.

REFERENCES

1. Morgan, K., Peraire, J., Thareja, R. R., and Stewart J. R., "An Adaptive Finite-Element Scheme for the Euler and Navier-Stokes Equations", *AIAA paper 87-1172, AIAA 8th Computational Fluid Dynamics Conference*, Honolulu, Hawaii, June, 1987.

2. Weatherill, N. P., Johnston, L. J., Peace, A. J., and Shaw, J. A., "A Method for the Solution of the Reynolds-Averaged Navier-Stokes Equations on Triangular Grids", *Proceedings of the 7th GAMM Conference on Numerical Methods in Fluids*, Louvain, Belgium, Sept, 1987.

3. Nakahashi, N., "FDM-FEM Zonal Approach for Viscous Flow Computations Over Multiple Bodies", *AIAA paper 87-0604*, January, 1987.

4. Mavriplis, D. J., Jameson, A. "Multigrid Solution of the Navier-Stokes Equations on Triangular Meshes", *AIAA Journal, Vol 28, No. 8, pp. 1415-1425* August, 1990.

5. Holmes, D. G., Connell, S. D., "Solution of the 2D Navier-Stokes Equations on Unstructured Adaptive Grids", *Paper presented at the AIAA 9th Computational Fluid Dynamics Conference*, June, 1989

6. Baldwin, B. S., Lomax, H., "Thin Layer Approximation and Algebraic Model for Separated Turbulent Flows", *AIAA paper 78-275*, 1978

7. Mavriplis, D. J., "Algebraic Turbulence Modeling for Unstructured and Adaptive Meshes" *AIAA paper 90-1653*, June, 1990.

8. Dimitriadis, K. P., Leschziner, M. A., "Multilevel Convergence Acceleration for Viscous and Turbulent Transonic Flows Computed with a Cell-Vertex Method" *Proceedings of the Fourth Copper Mountain Conference on Multigrid Methods*, Copper Mountain, Colorado, April 9-14, 1989, Eds. J. Mandel, S. McCormick, J. Dendy, G. Lonsdale, S. Parter, J. Ruge, K. Stuben, SIAM Publications

9. Gerolymos, G. A., "Implicit Multiple-Grid Solution of the Compressible Navier-Stokes Equations Using $k - \varepsilon$ Turbulence Closure" *AIAA Journal, Vol 28, No. 10, pp. 1707-1717* October, 1990.

10. Mavriplis, D. J., "Multigrid Solution of the Two-Dimensional Euler Equations on Unstructured Triangular Meshes", *AIAA Journal*, Vol 26, No. 7, July 1988, pp. 824-831

11. Launder, B. E. , Spalding, D. B., "The Numerical Computation of Turbulent Flows", *Computer Methods in Applied Mechanics and Engineering*, Vol 3, pp. 269-289, 1974

12. Martinelli, L., "Calculations of Viscous Flows with a Multigrid Method" *Ph.D Thesis*, Department of Mechanical and Aerospace Engineering, Princeton University, October, 1987.

13. Martinelli, L., and Jameson, A., "Validation of a Multigrid Method for the Reynolds Averaged Equations" *AIAA paper 88-0414*, January 1988.

14. Cook, P. H., McDonald, M. A., and Firmin, M. C. P., "Aerofoil RAE 2822 Pressure Distributions and Boundary Layer and Wake Measurements", *AGARD Advisory Report No. 138* May 1979.

15. Coakley, T. J., "Numerical Simulation of Viscous Transonic Airfoil Flows", *AIAA paper 87-0416* January 1987.

16. Omar, E. , Zierten, T., Hahn, M., Szpizo, E., and Mahal, A., "Two-Dimensional Wind-Tunnel Tests of a NASA Supercritical Airfoil with Various High-Lift Systems, Volume II - Test Data", *NASA CR-2215*, April, 1977.

17. Patel, V. C., Rodi, W., and Scheuerer, G., "Turbulence Models for Near-Wall and Low Reynolds Number Flows: A Review", *AIAA Journal, Vol, 23, pp. 1308-1319*, September, 1985.

18. Speziale, C. G., Abid, R., and Anderson, E. C., "A Critical Evaluation of Two-Equation Models for Near Wall Turbulence", *ICASE Report 90-46, NASA CR 182068, AIAA paper 90-1481*, June, 1990

19. Lam, C. K. G., and Bremhorst, K., "A Modified Form of the $k - \varepsilon$ Model for Predicting Wall Turbulence", *Journal of Fluids Engineering, Vol. 103, pp. 456-460*, 1981

20. Barth, T. J., "Numerical Aspects of Computing Viscous High-Reynolds Number Flows on Unstructured Meshes", *AIAA paper 91-0721* January, 1991.

21. Mansour, N. N., Kim, J. and Moin, P., "Reynolds Stress and Dissipation Rate Budgets in Turbulent Channel Flow", *Journal of Fluid Mechanics, Vol. 194, pp. 15-44* September, 1988

22. Kim, J., Moin, P., and Moser, R., "Turbulence Statistics in Fully Developed Channel Flow at low Reynolds Number", I. Journal of Fluid Mechanics, Vol 177, pp 133,166 April, 1987

23. Wieghardt, K. and Tillmann, W., "On the Turbulent Friction Layer for Rising Pressure", *NACA TM 1314*, 1951

24. Volpe, G., "A Multigrid Method for Computing the Transonic Flow Over Two Closely-Coupled Airfoil Components", *ICAS paper 84-1.4.3*, Paper presented at the 14th ICAS Congress, Toulouse, France, September, 1984.

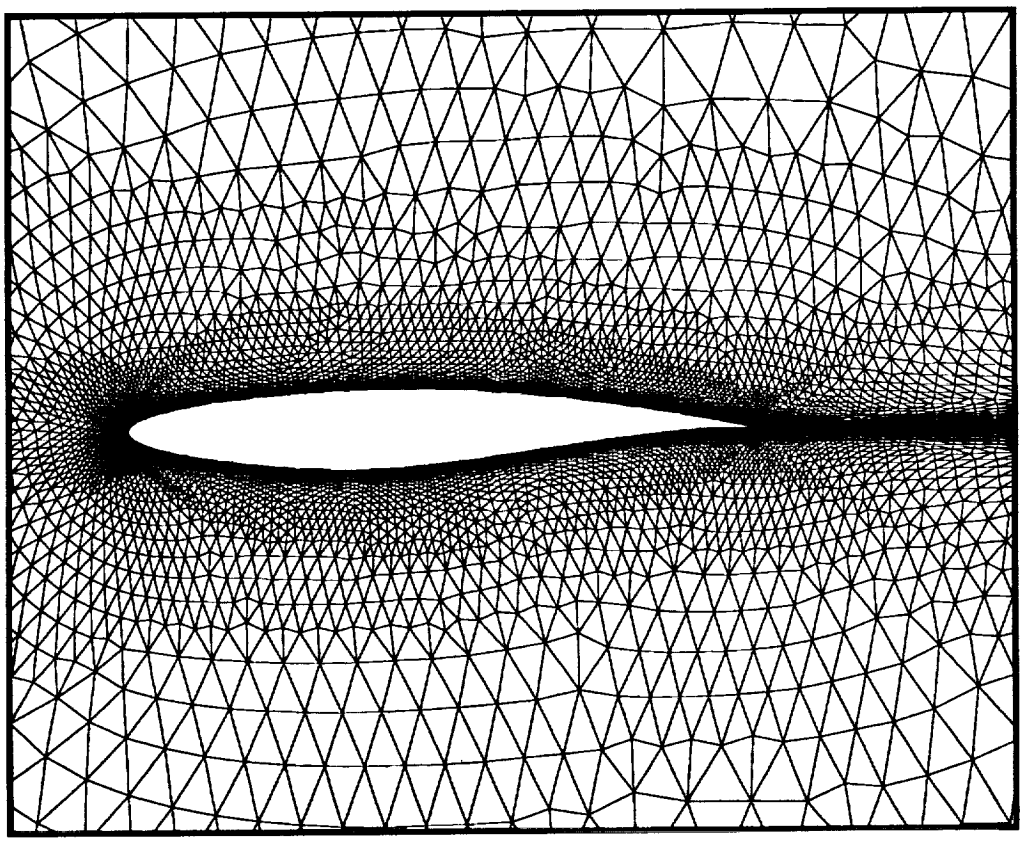

Figure 1
Unstructured Mesh Employed for Computing Flow Over an RAE 2822 Airfoil
(Number of Vertices = 12,823)

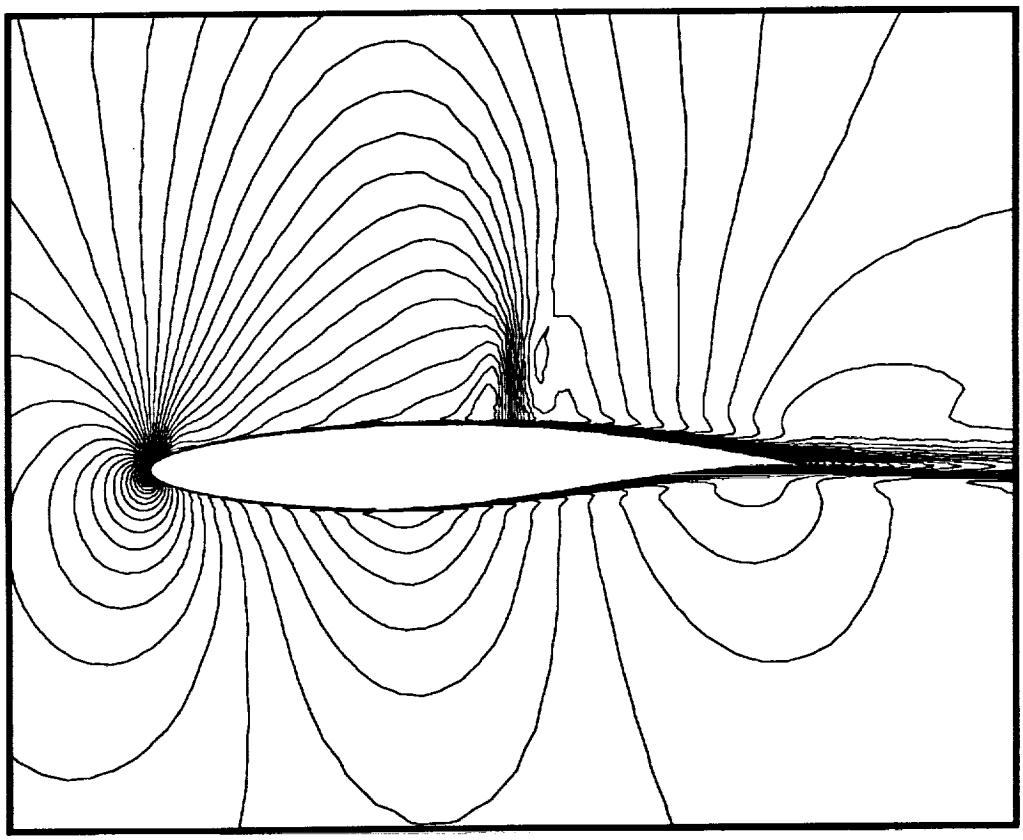

Figure 2
Computed Mach Contours for Turbulent Flow over RAE 2822 Airfoil
Using Wall Functions (Mach = 0.729, Re = 6.5 million, Incidence = 2.31 degrees)

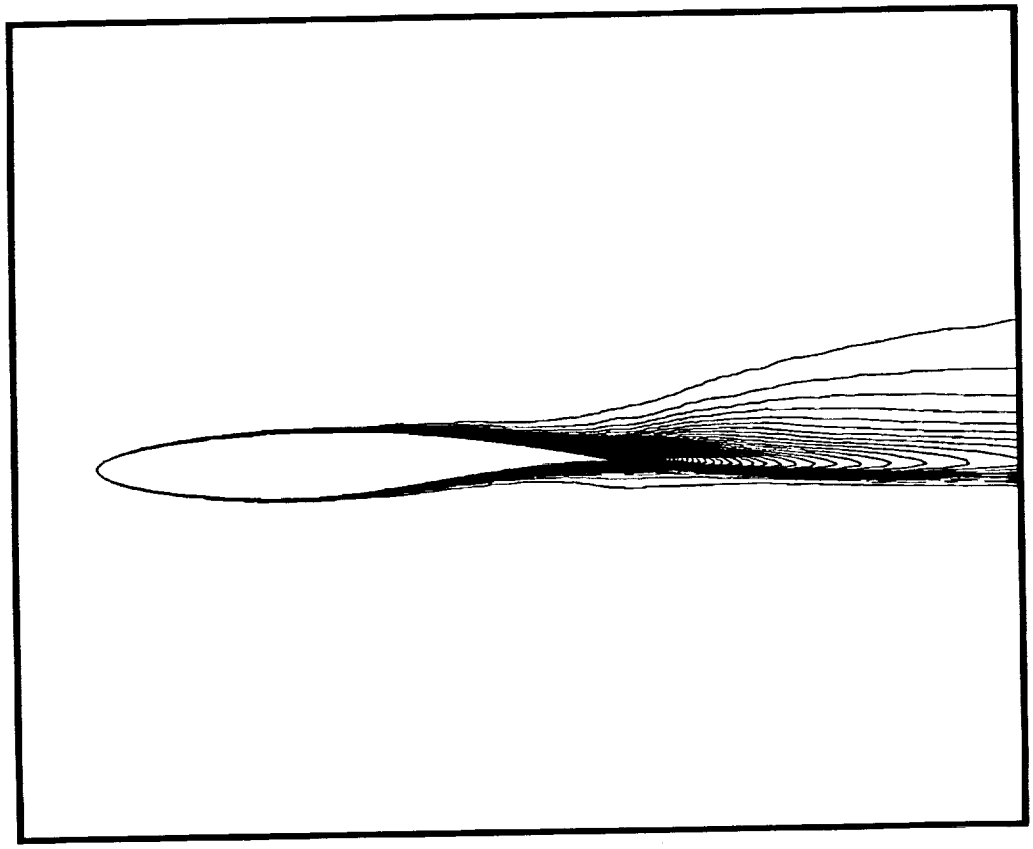

Figure 3
Computed Eddy Viscosity Contours for Turbulent Flow over RAE 2822 Airfoil
Using Wall Functions (Mach = 0.729, Re = 6.5 million, Incidence = 2.31 degrees)

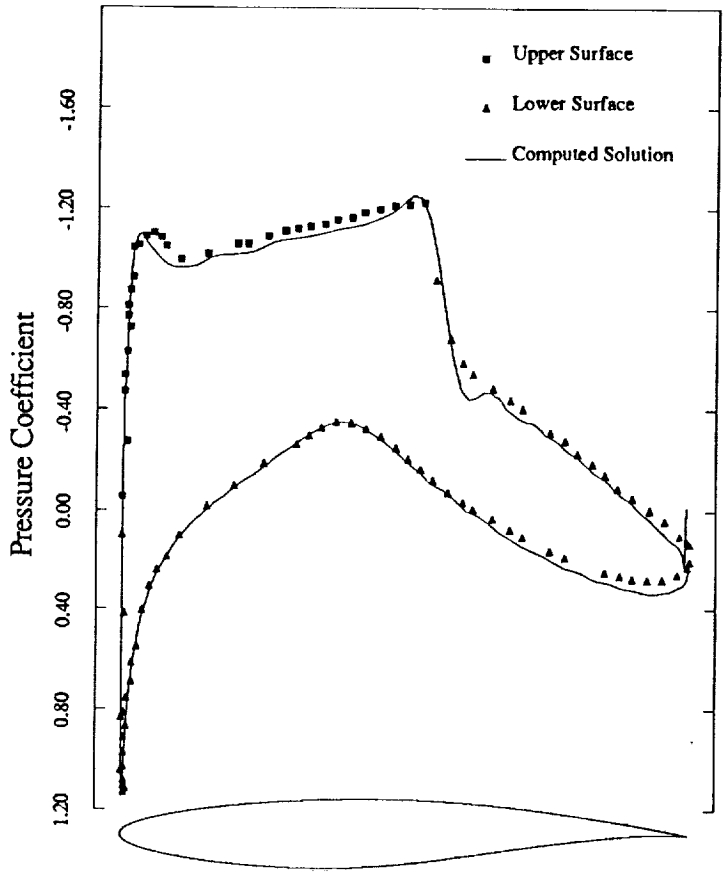

Figure 4
Comparison of Computed Surface Pressure using Wall Functions with Experimental Measurements for Flow over an RAE 2822 Airfoil
(Mach = 0.729, Re = 6.5 million, Incidence = 2.31 degrees)

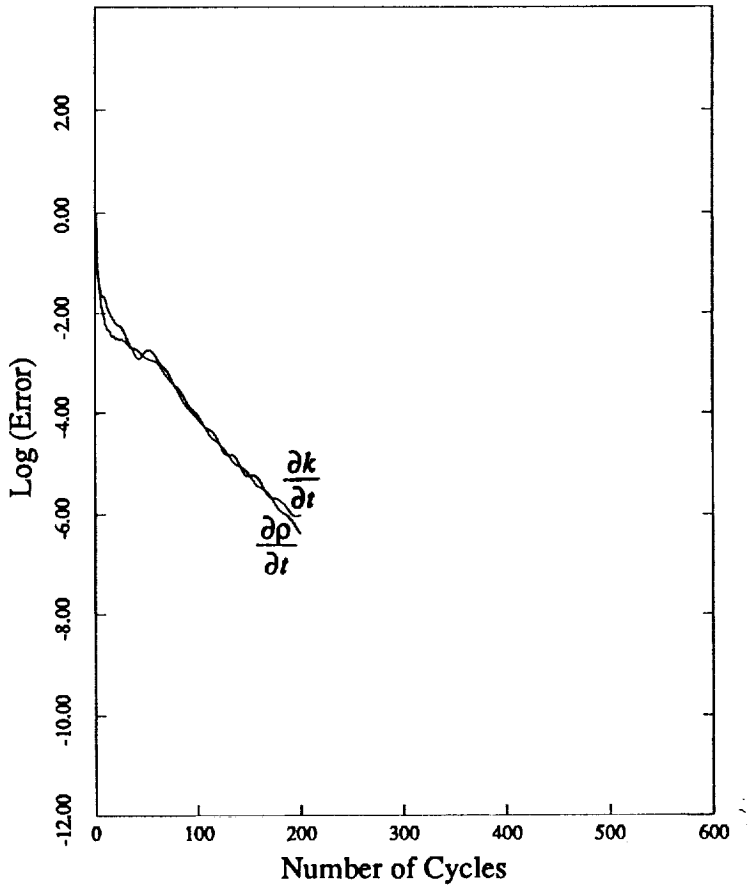

Figure 5
Convergence Rate of Density Equation and K equation Using Wall Functions versus the Number of Multigrid Cycles for Flow over an RAE 2822 Airfoil

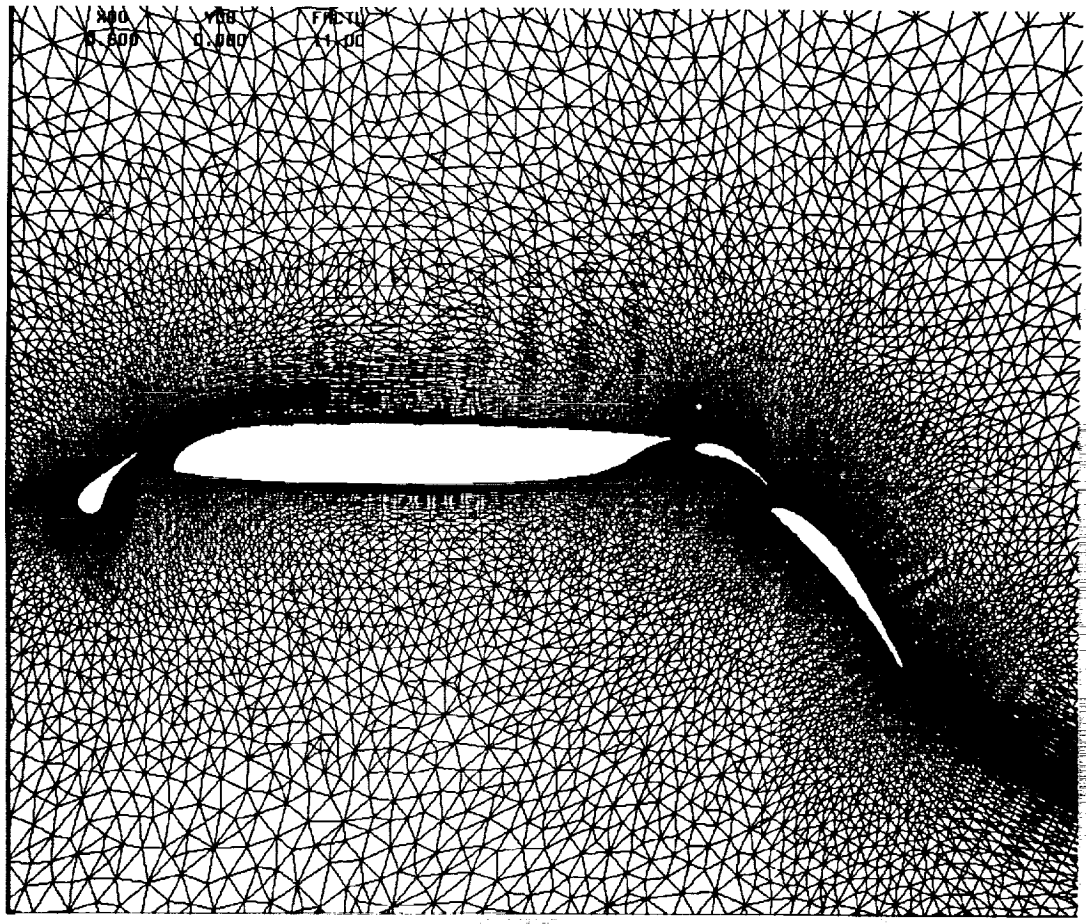

Figure 6
Unstructured Mesh Employed for Computing Flow Over a Four-Element Airfoil
(Number of Vertices = 51,100)

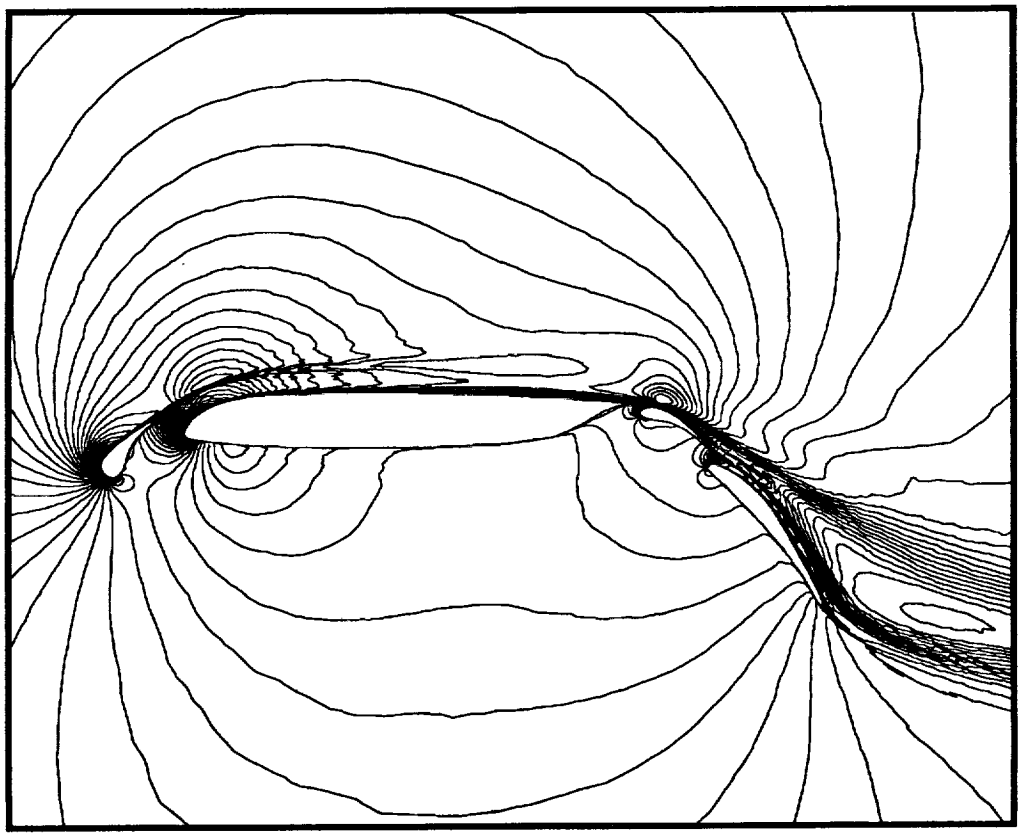

Figure 7
Computed Mach Contours Using Wall Functions for Flow over a Four-Element Airfoil
(Mach = 0.2, Re = 2.83 million, Incidence = 8.18 degrees)

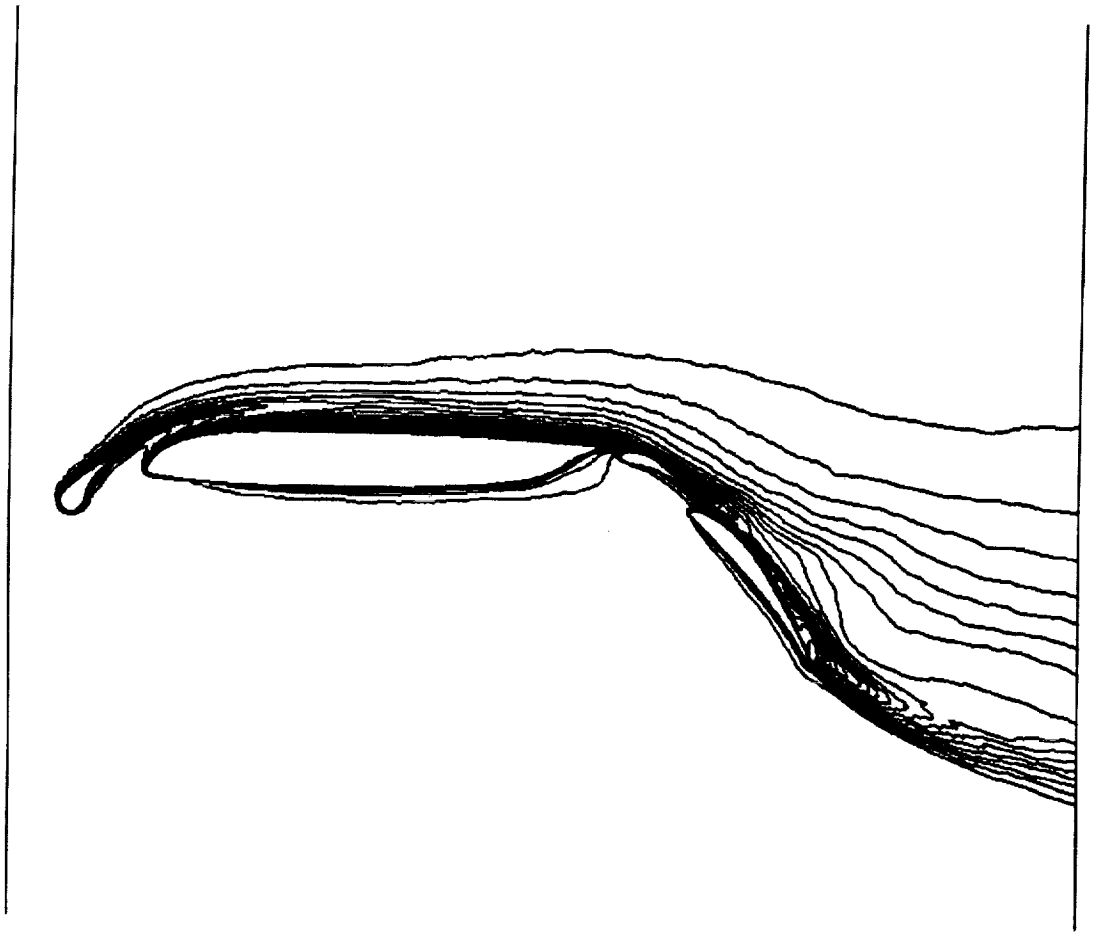

Figure 8
Computed Eddy Viscosity Contours Using Wall Functions for Flow over a Four-Element Airfoil
(Mach = 0.2, Re = 2.83 million, Incidence = 8.18 degrees)

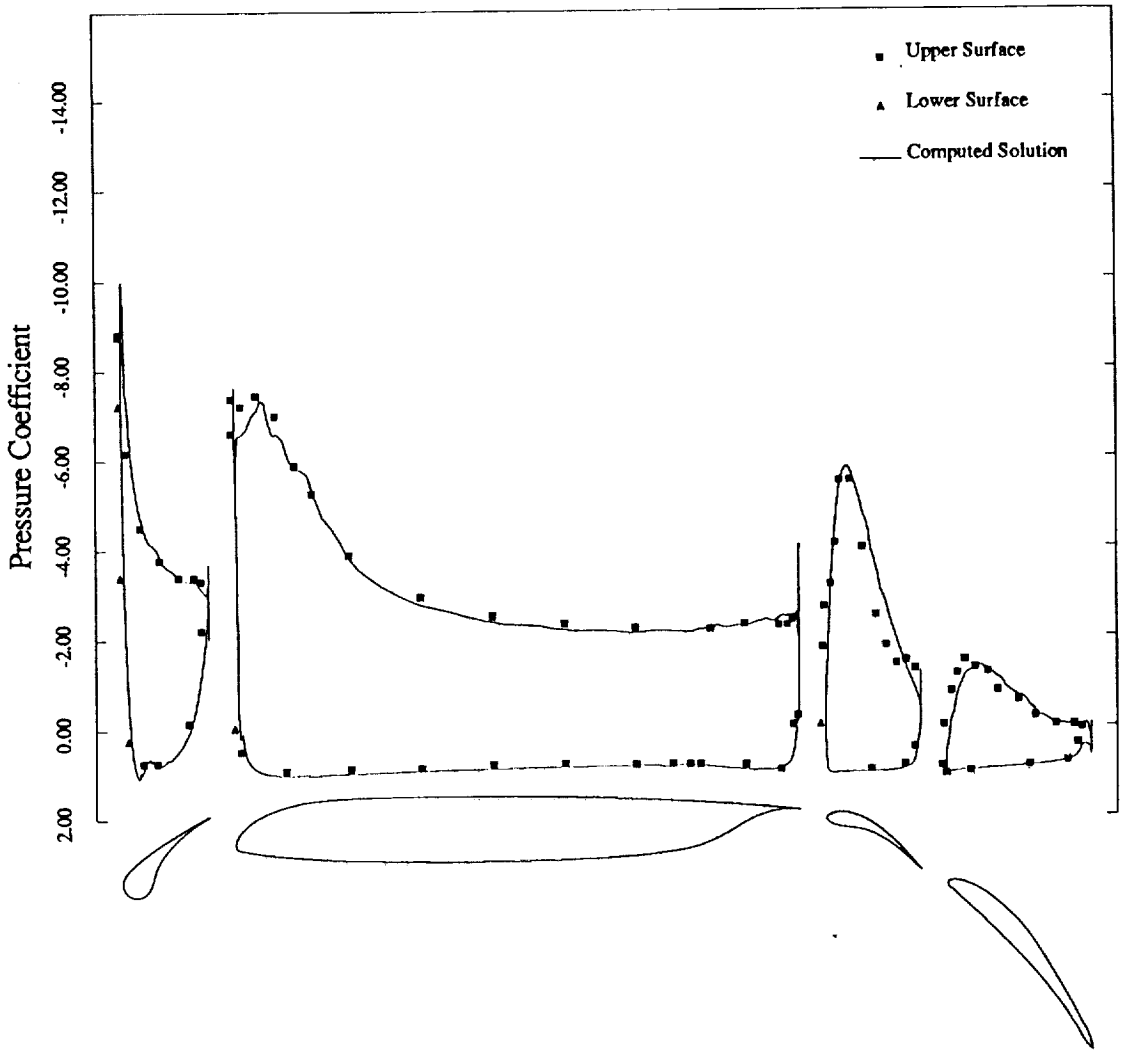

Figure 9
Comparison of Computed Surface Pressure using Wall Functions with Experimental Wind-Tunnel Data for Flow over a Four-Element Airfoil
(Mach = 0.2, Re = 2.83 million, Incidence = 8.18 degrees)

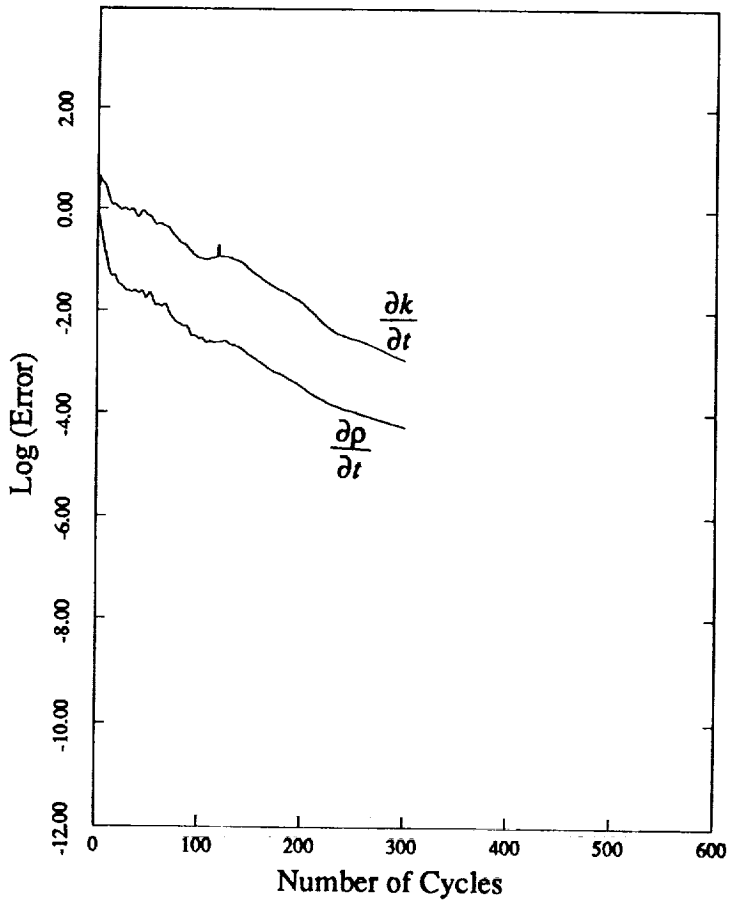

Figure 10
Multigrid Convergence Rate of Density Equation and K Equation Using Wall Functions for Flow over a Four-Element Airfoil

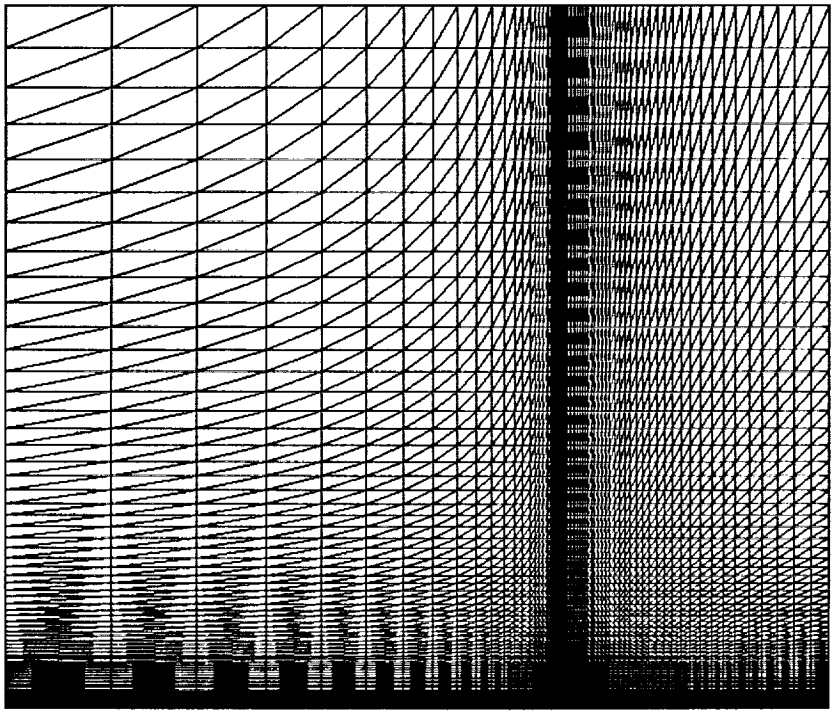

Figure 11
Triangular Mesh Employed for Flat Plate Boundary Layer Calculation
(Number of Vertices = 5913, 10:1 Magnification in Y-direction)

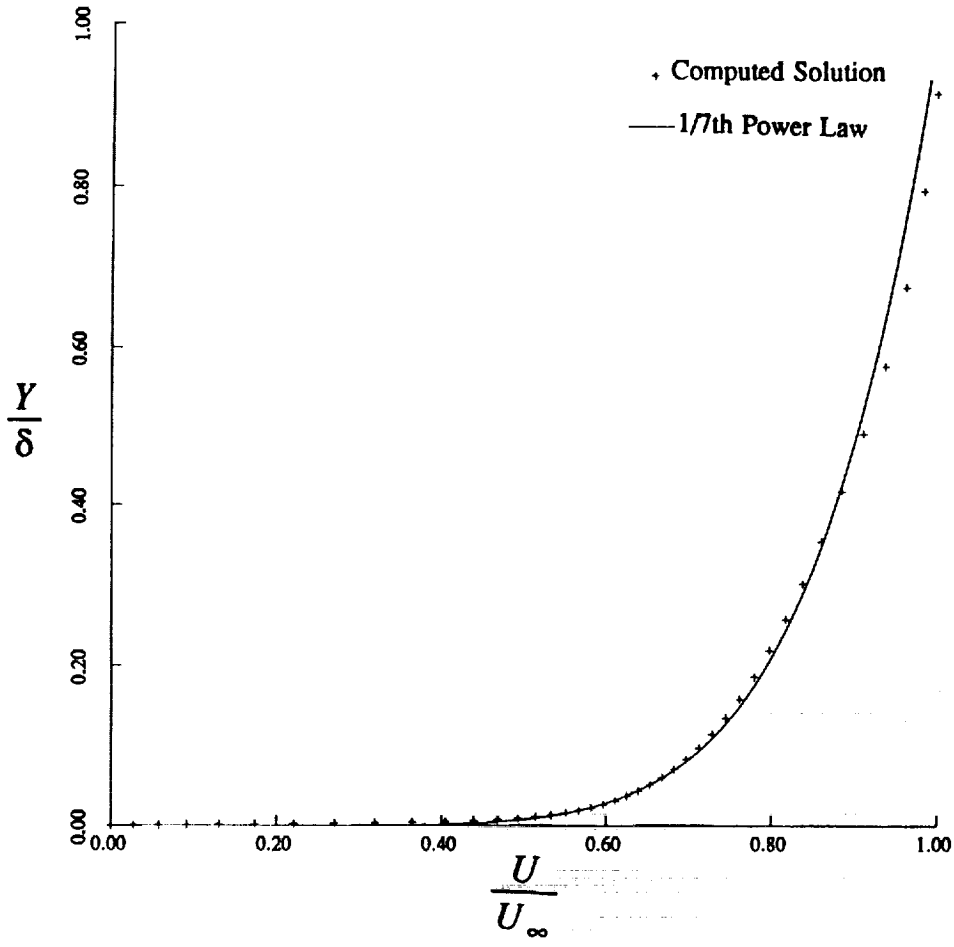

Figure 12
Computed Velocity Profile in Physical Coordinates Versus the 1/7th Power Law Profile
(Mach = 0.3, Re_x = 5.3 million)

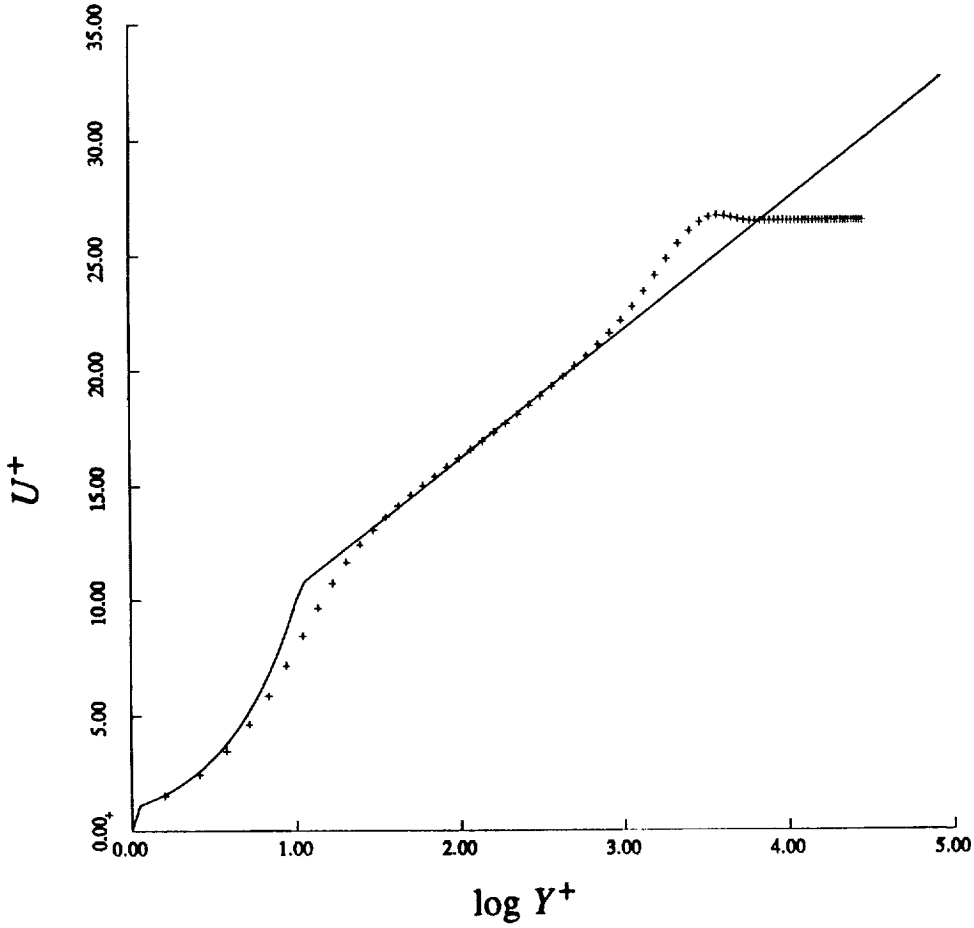

Figure 13
Computed Velocity Profile in Logarithmic Coordinates Versus Logarithmic Law of the Wall
(Mach = 0.3, Re_x = 5.3 million)

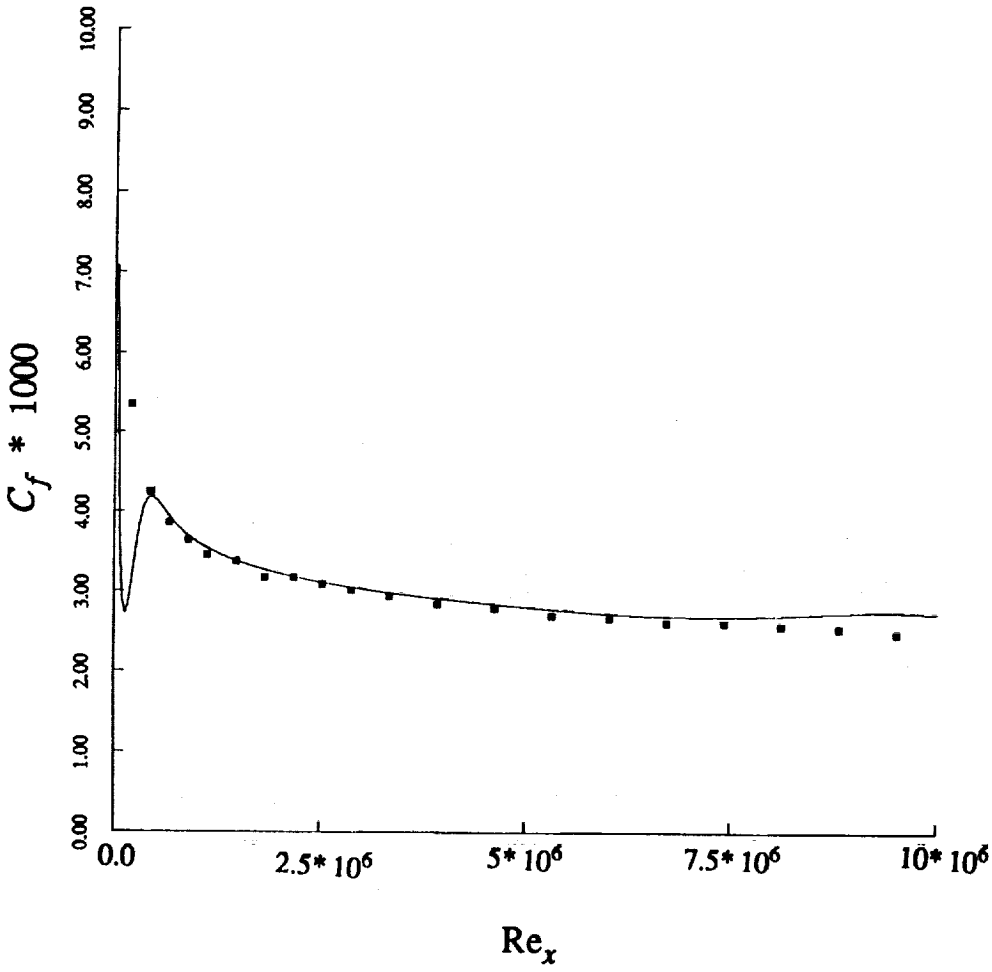

Figure 14
Computed Skin Friction Distribution for Flat Plate Boundary Layer
Versus Experimental Data from [23]

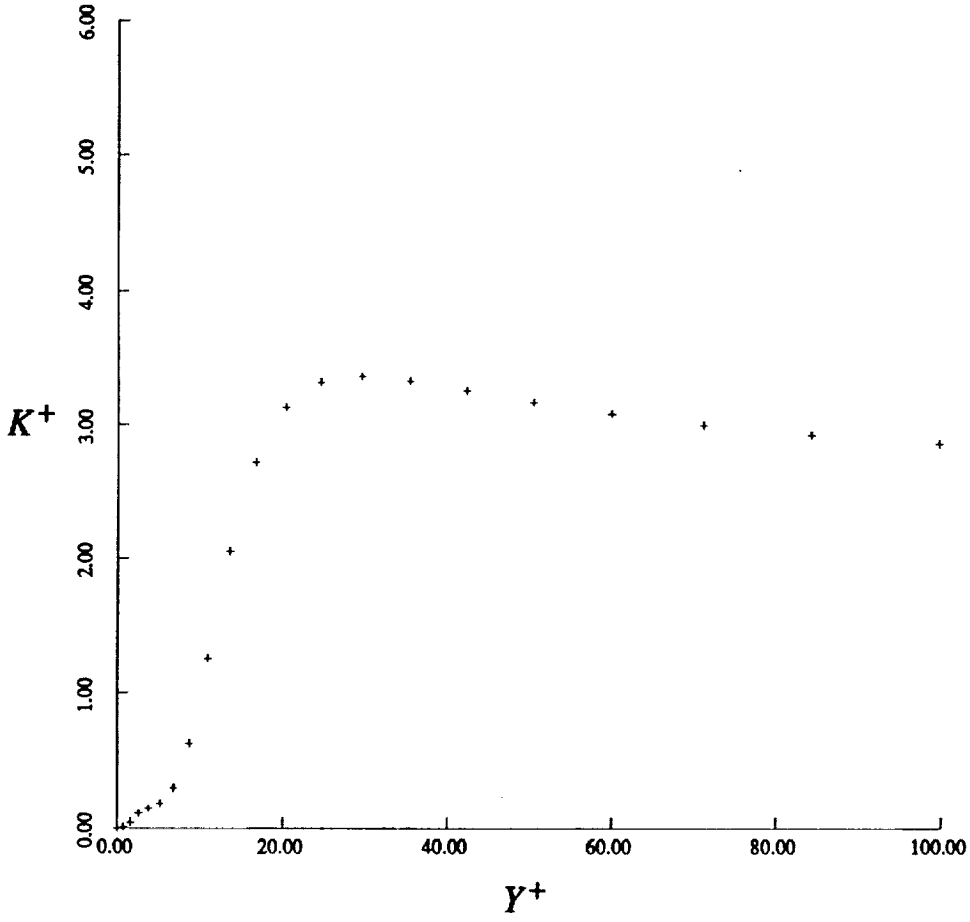

Figure 15
Computed Near Wall Distribution of k^+ for Flat Plate Boundary Layer
(Mach = 0.3, Re_x = 5.3 million)

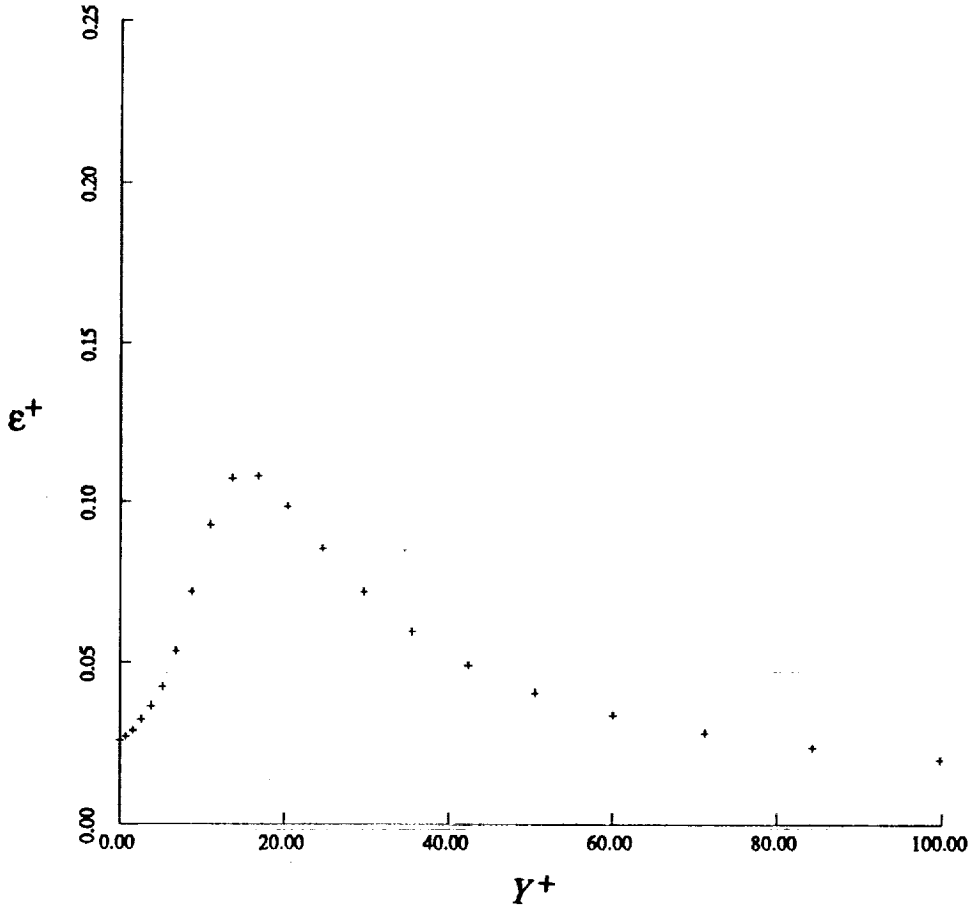

Figure 16
Computed Near Wall Distribution of ε^+ for Flat Plate Boundary Layer
(Mach = 0.3, Re_x = 5.3 million)

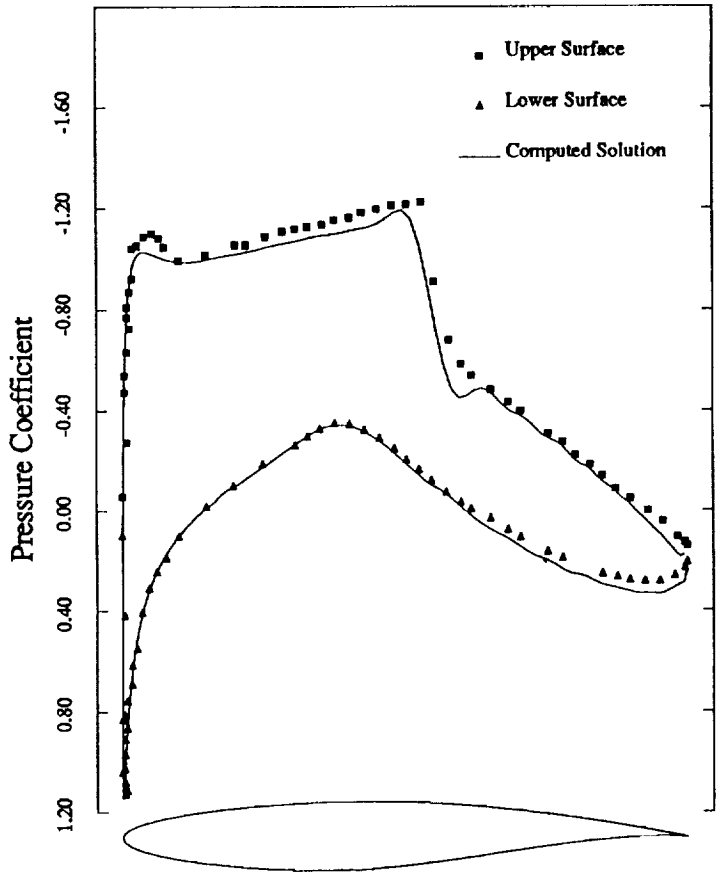

Figure 17
Computed Surface Pressure Distribution Using Low-Reynolds Number Modification for Turbulence Equations Versus Experimental Data for Flow past RAE 2822 Airfoil (Mach = 0.729, Re = 6.5 million, Incidence = 2.31 degrees)

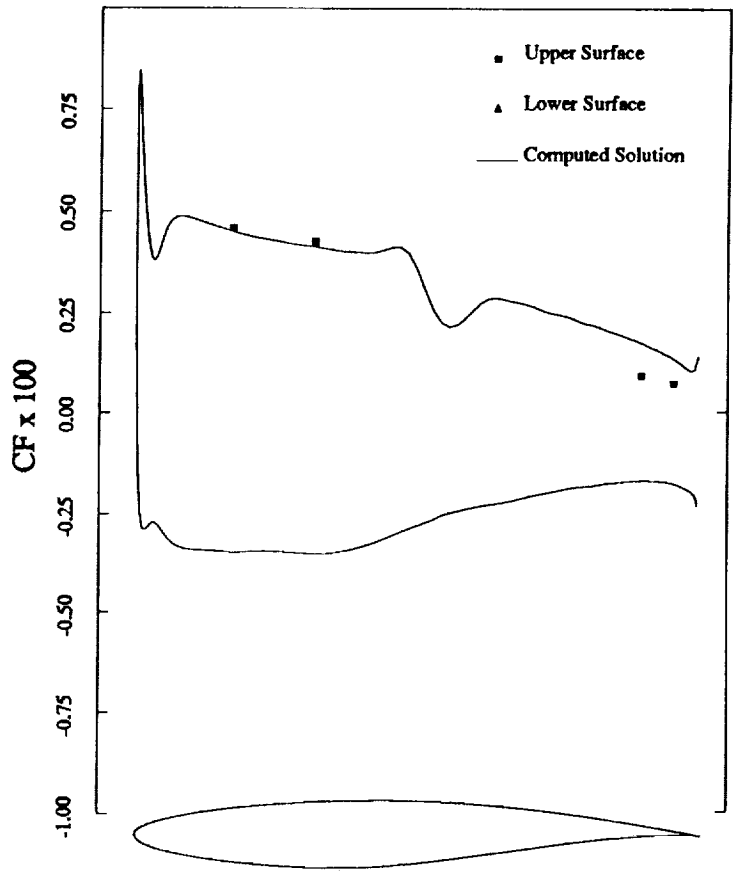

Figure 18
Computed Skin-Friction Distribution Using Low-Reynolds Number Modification for Turbulence Equations Versus Experimental Data for Flow past RAE 2822 Airfoil (Mach = 0.729, Re = 6.5 million, Incidence = 2.31 degrees)

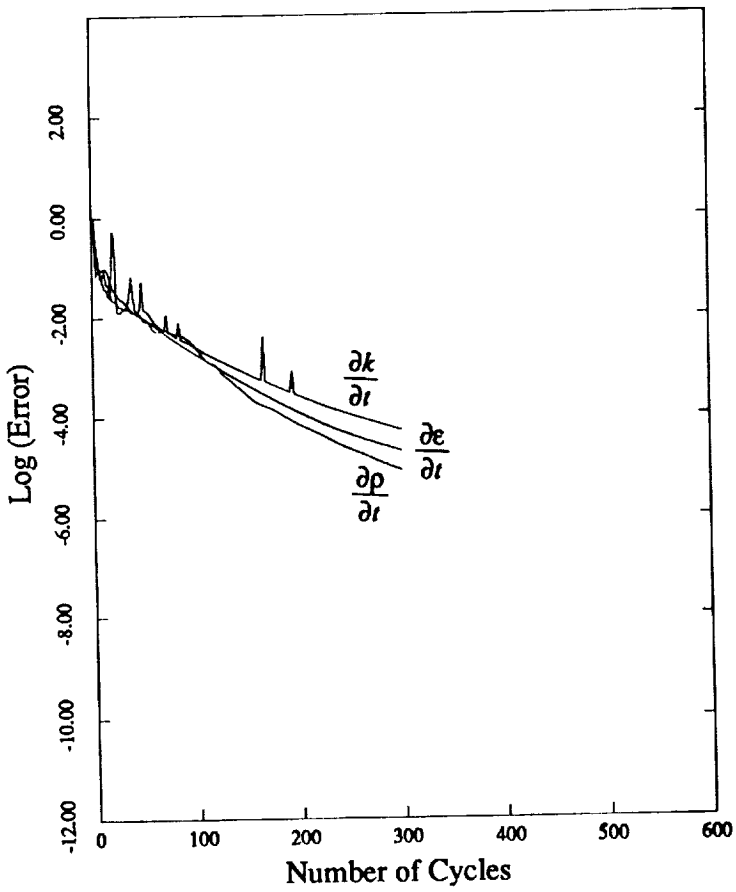

Figure 19
Convergence Rate of the Density Equation and the Two Turbulence Equations
Modified for Low-Reynolds Number Effects Versus the Number of Multigrid Cycles for Flow Past RAE 2822 Airfoil

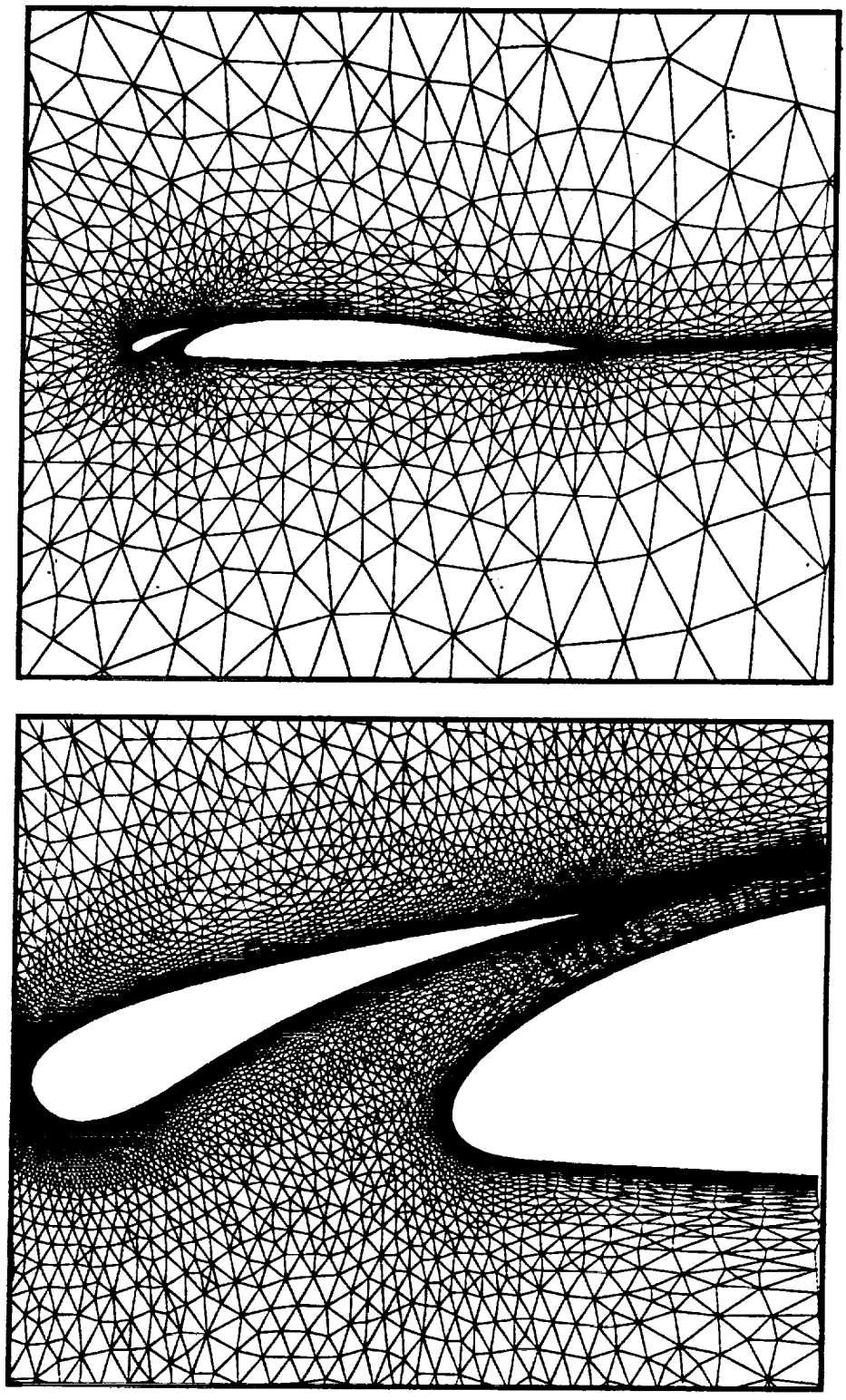

Figure 20
Global View of Coarse Unstructured Mesh and Close-Up View of Fine Unstructured Mesh Employed for Computing Flow Past a Two-Element Airfoil (Coarse Mesh Points = 7272, Fine Mesh Points = 28871)

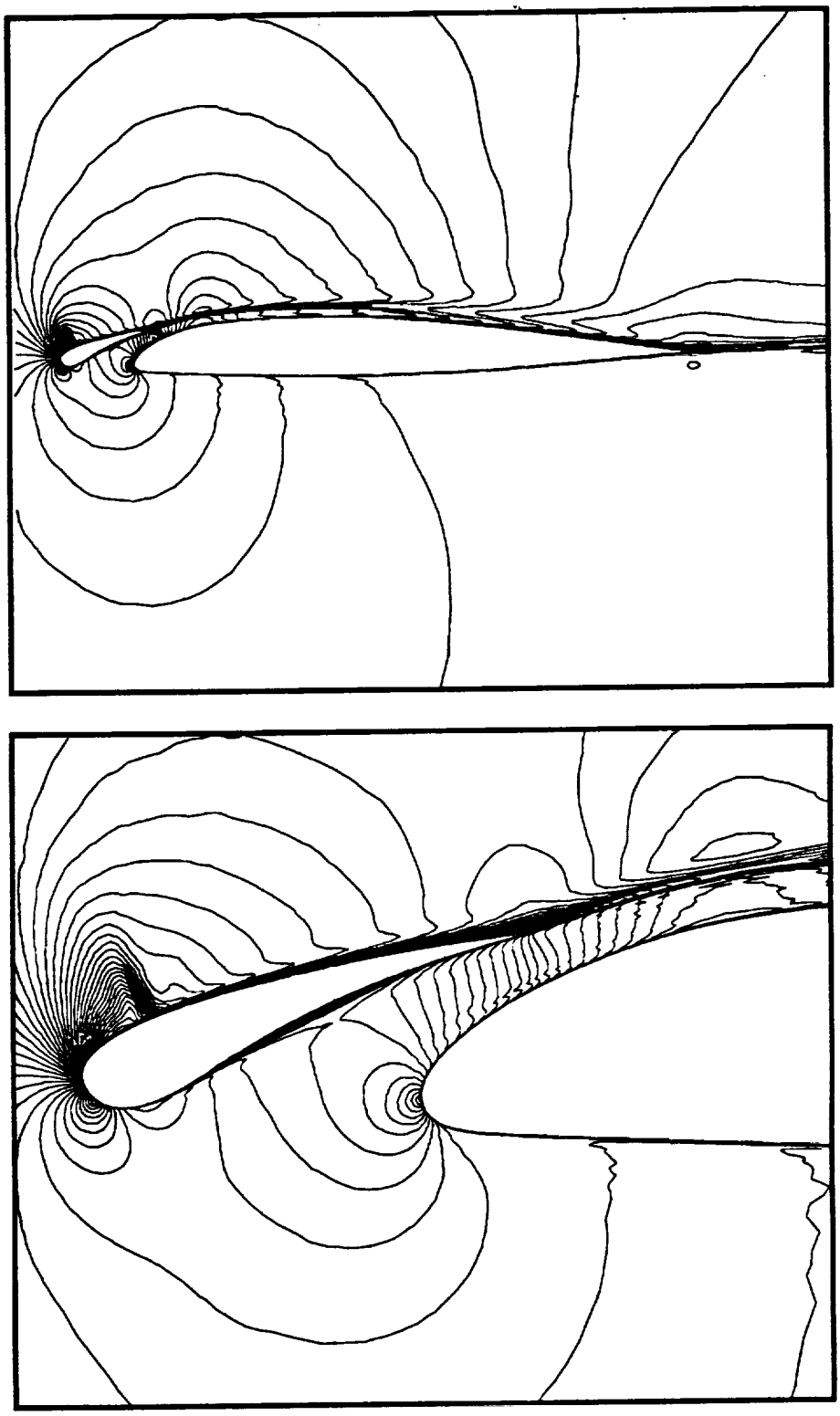

Figure 21
Computed Mach Contours Using Low-Reynolds Number Modification for Turbulence Equations for Supercritical Flow over a Two-Element Airfoil
(Mach = 0.5, Re = 4.5 million, Incidence = 7.5 degrees)

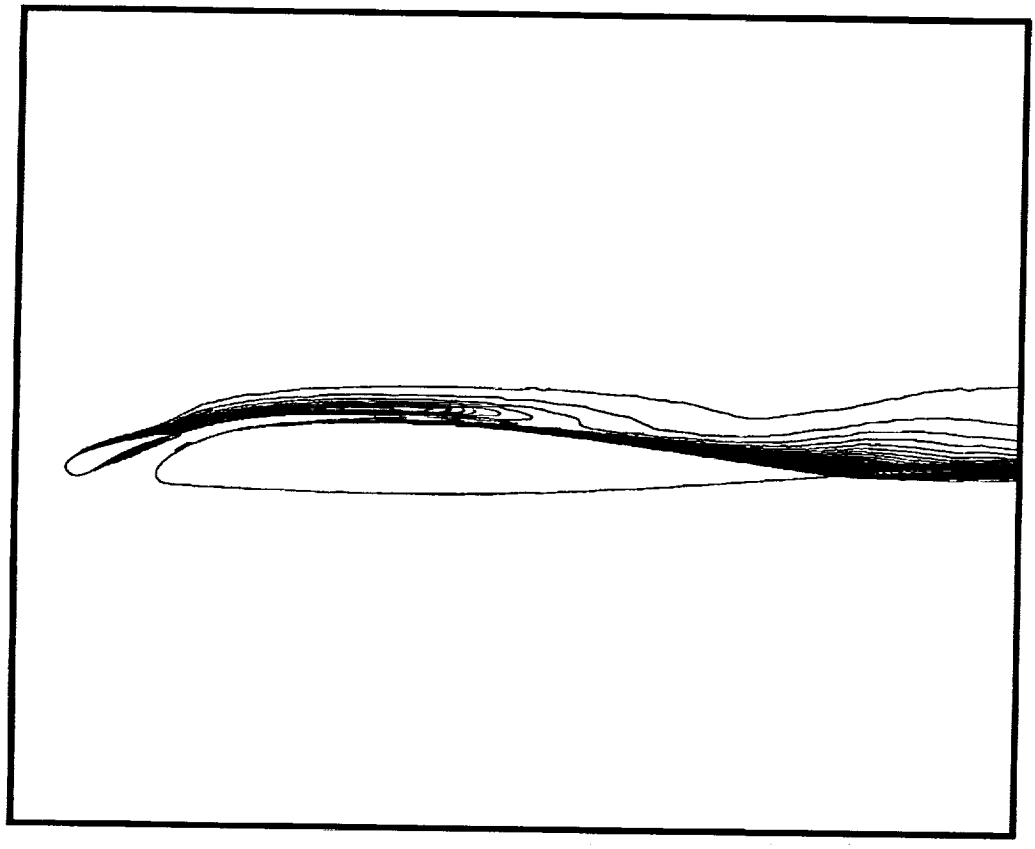

Figure 22
Computed Eddy Viscosity Contours Using Low-Reynolds Number Modification for Turbulence Equations for Supercritical Flow over a Two-Element Airfoil (Mach = 0.5, Re = 4.5 million, Incidence = 7.5 degrees)

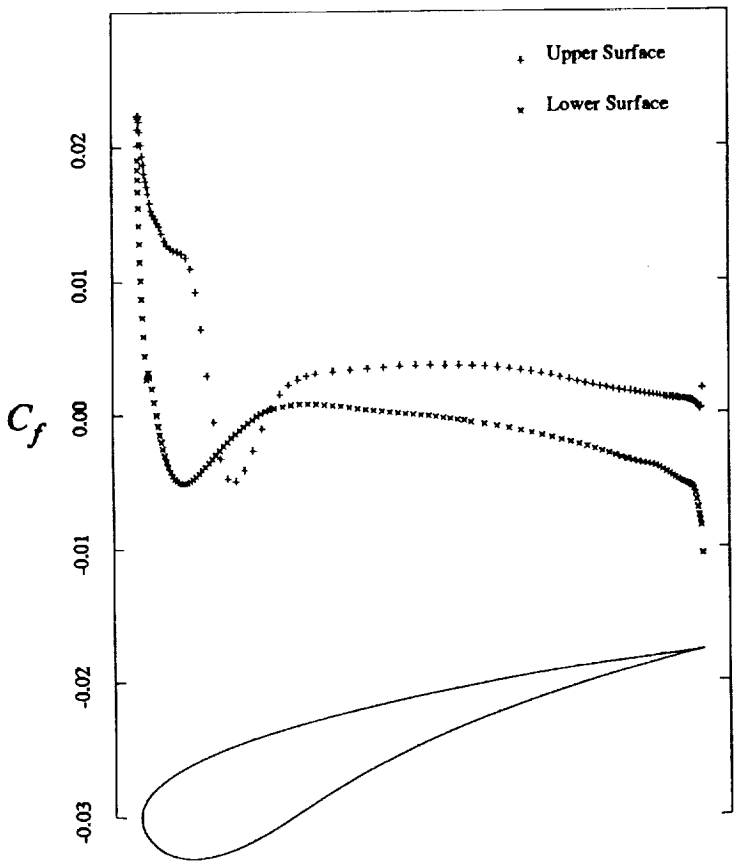

Figure 23
Computed Skin-Friction Distribution on Slat Showing Region of Separated Flow Behind Upper Surface Shock (Mach = 0.5, Re = 4.5 million, Incidence = 7.5 degrees)

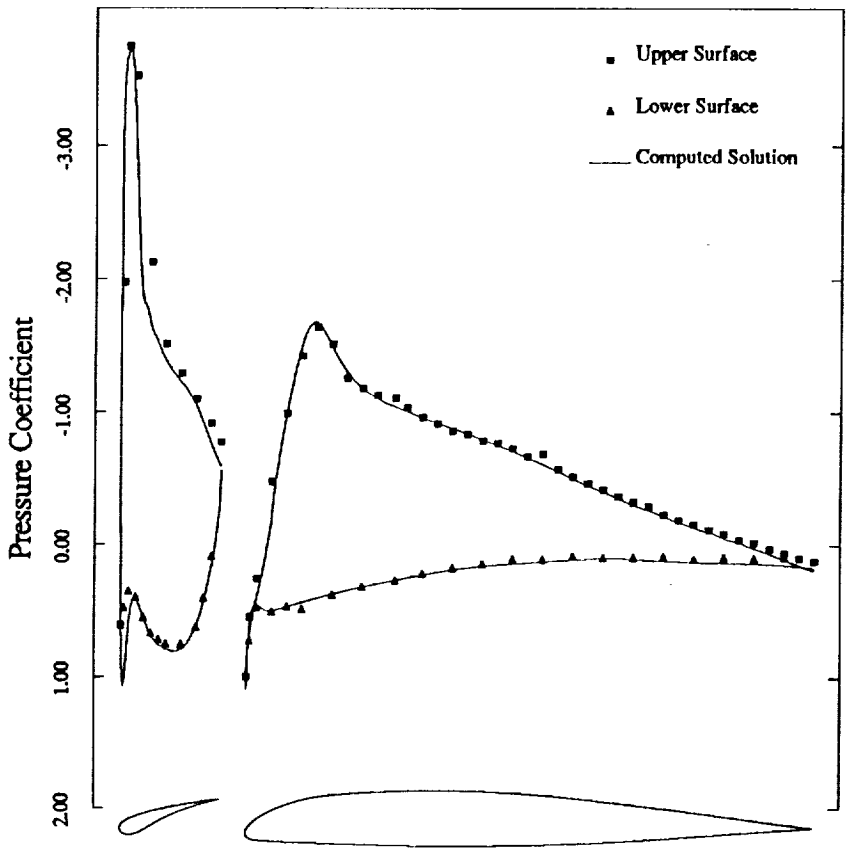

Figure 24
Computed Surface Pressure Distribution Using Low-Reynolds Number Modification for Turbulence Equations for Supercritical Flow over a Two-Element Airfoil Versus Experimental Wind Tunnel Data
(Mach = 0.5, Re = 4.5 million, Incidence = 7.5 degrees)

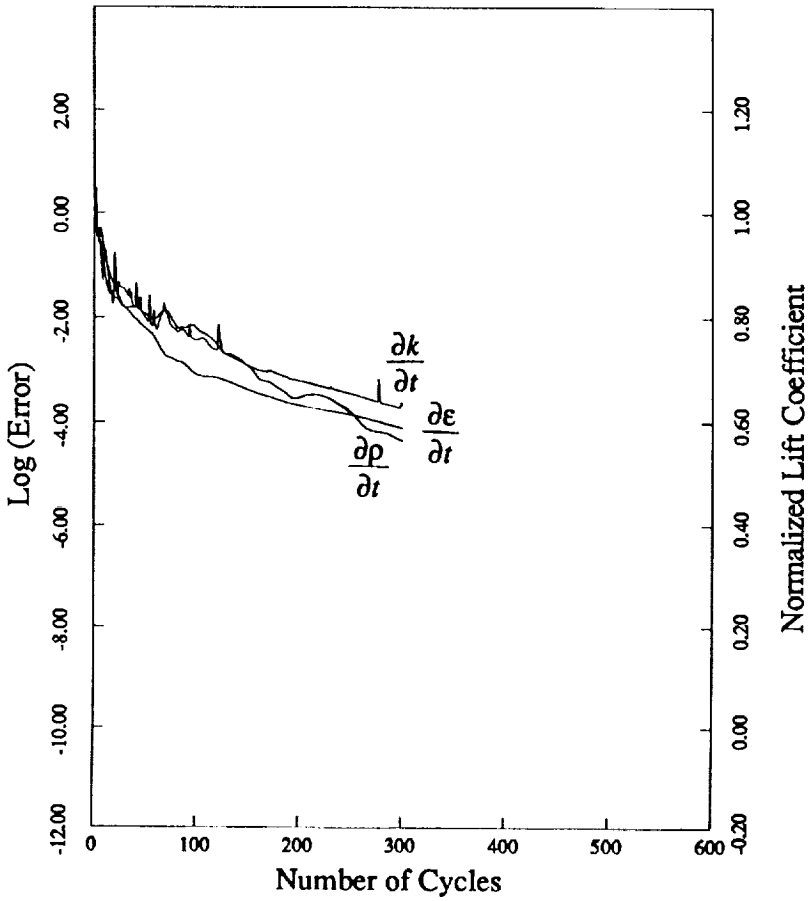

Figure 25
Multigrid Convergence Rate of the Density Equation and the Two Turbulence Equations Using Low-Reynolds Number Modifications for Flow Over Two-Element Airfoil (Mach = 0.5, Re = 4.5 million, Incidence = 7.5 degrees)

NASA
National Aeronautics and Space Administration

Report Documentation Page

1. Report No.	2. Government Accession No.	3. Recipient's Catalog No.
NASA CR-187513 ICASE Report No. 91-11		

4. Title and Subtitle

MULTIGRID SOLUTION OF COMPRESSIBLE TURBULENT FLOW ON UNSTRUCTURED MESHES USING A TWO-EQUATION MODEL

5. Report Date

January 1991

6. Performing Organization Code

7. Author(s)

D. J. Mavriplis
L. Martinelli

8. Performing Organization Report No.

91-11

10. Work Unit No.

505-90-52-01

9. Performing Organization Name and Address

Institute for Computer Applications in Science and Engineering
Mail Stop 132C, NASA Langley Research Center
Hampton, VA 23665-5225

11. Contract or Grant No.

NAS1-18605

13. Type of Report and Period Covered

Contractor Report

12. Sponsoring Agency Name and Address

National Aeronautics and Space Administration
Langley Research Center
Hampton, VA 23665-5225

14. Sponsoring Agency Code

15. Supplementary Notes

Langley Technical Monitor:
Michael F. Card

Submitted to AIAA Journal

Final Report

16. Abstract

The system of equations consisting of full Navier-Stokes equations and two turbulence equations has been solved for in the steady-state using a multigrid strategy on unstructured meshes. The flow equations and turbulence equations are solved in a loosely coupled manner. The flow equations are advanced in time using a multi-stage Runge-Kutta time stepping scheme with a stability bound local time-step, while the turbulence equations are advanced in a point-implicit scheme with a time-step which guarantees stability and positivity. Low Reynolds number modifications to the original two-equation model are incorporated in a manner which flows are solved for, initializing all quantities with uniform freestream values, and resulting in rapid and uniform convergence rates for the flow and turbulence equations.

17. Key Words (Suggested by Author(s))	18. Distribution Statement
multigrid, turbulence, unstructured	02 - Aerodynamics 34 - Fluid Mechanics and Heat Transfer Unclassified - Unlimited

19. Security Classif. (of this report)	20. Security Classif. (of this page)	21. No. of pages	22. Price
Unclassified	Unclassified	41	A03

NASA FORM 1626 OCT 86